UNIVERSITY OF COPENHAGEN



Københavns Universitet

Dihydrotanshinone as a Natural Product-Based CYP17A1 Lyase Inhibitor for Hyperandrogenic Disorders

Li, Kaige; Yakubu, Jibira; Jørgensen, Flemming Steen; Pandey, Amit V.

Published in:
Biomolecules

DOI:
10.3390/biom16010144

Publication date:
2026

Document version
Publisher's PDF, also known as Version of record

Document license:
CC BY

Citation for published version (APA):
Li, K., Yakubu, J., Jørgensen, F. S., & Pandey, A. V. (2026). Dihydrotanshinone as a Natural Product-Based CYP17A1 Lyase Inhibitor for Hyperandrogenic Disorders. *Biomolecules*, *16*(1), Article 144. https://doi.org/10.3390/biom16010144

Download date: 30. Sep. 2026

biomolecules

MDPI

Article

Dihydrotanshinone as a Natural Product-Based CYP17A1 Lyase Inhibitor for Hyperandrogenic Disorders

Kaige Li [1,2,3,†], Jibira Yakubu [1,2,3,†], Flemming Steen Jørgensen [4,*] and Amit V. Pandey [1,2,*]

[1] Pediatric Endocrinology, Diabetology and Metabolism, University Children's Hospital, Inselspital, CH-3010 Bern, Switzerland
[2] Translational Hormone Research Program, Department of Biomedical Research, Faculty of Medicine, University of Bern, CH-3010 Bern, Switzerland
[3] Graduate School for Cellular and Biomedical Sciences, University of Bern, CH-3012 Bern, Switzerland
[4] Department of Drug Design and Pharmacology, University of Copenhagen, DK-2100 Copenhagen, Denmark
* Correspondence: fsj@sund.ku.dk (F.S.J.); amit.pandey@unibe.ch (A.V.P.); Tel.: +45-353-36378 (F.S.J.); +41-31-632-9637 (A.V.P.)
† These authors contributed equally to this work.

Abstract

Selective inhibition of CYP17A1 17,20-lyase is critical for treating hyperandrogenic disorders without the cortisol-depleting side effects of non-selective drugs like abiraterone. We evaluated tanshinones from *Salvia miltiorrhiza* as potential selective inhibitors using biochemical assays and computational modeling. Dihydrotanshinone (DT) emerged as the superior candidate; at 10 μM, it inhibited 17,20-lyase activity by 56.6% while preserving >93% of 17α-hydroxylase activity. This yields a selectivity index of 8.67, drastically outperforming abiraterone (0.73). Furthermore, DT displayed minimal off-target inhibition of CYP21A2 (14.9%) compared to abiraterone (29.8%). Molecular modeling suggests DT's efficacy arises from a unique, functionally disruptive binding pose rather than superior thermodynamic affinity. Consequently, DT is validated as a potent natural product lead. Its dual selectivity over 17α-hydroxylase and CYP21A2 establishes the tanshinone scaffold as a promising candidate for developing safer therapies that suppress androgens while sparing cortisol biosynthesis.

Keywords: CYP17A1; 17α-hydroxylase; CYP17A1 lyase; CYP21A2; steroidogenesis; hyperandrogenism; PCOS; selective inhibition

Check for updates

Academic Editor: Philippe Urban

Received: 2 December 2025
Revised: 5 January 2026
Accepted: 8 January 2026
Published: 14 January 2026

Copyright: © 2026 by the authors. Licensee MDPI, Basel, Switzerland. This article is an open access article distributed under the terms and conditions of the Creative Commons Attribution (CC BY) license.

1. Introduction

Hyperandrogenism, the excessive production of androgens, is a primary driver of common and debilitating endocrine disorders, most notably polycystic ovary syndrome (PCOS) affecting 5–26% of women worldwide. PCOS is a leading cause of reproductive and metabolic dysfunction in women of reproductive age [1]. It is characterized by hyperandrogenism, menstrual irregularities, and polycystic ovarian morphology. Clinical manifestations include acne, alopecia, hirsutism, infertility, obesity, insulin resistance, and increased risk of cardiovascular disease, anxiety, and depression [2,3]. Similarly in congenital adrenal hyperplasia, elevated androgen levels are a constant challenge. Hyperandrogenism in PCOS is driven by dysregulated steroidogenesis, particularly overactivity of cytochrome P450 17A1 (CYP17A1) in ovarian theca cells. CYP17A1 is a dual-function enzyme with 17α-hydroxylase and 17,20-lyase activities, catalyzing key steps in the synthesis of dehydroepiandrosterone (DHEA) and androstenedione, precursors of testosterone [4–6]

(Figure 1). Overexpression or increased activity of CYP17A1 due to changes in redox partner availability or protein phosphorylation leads to excessive androgen production, amplifying PCOS symptoms [7–9]. In contrast, CYP21A2 primarily regulates glucocorticoid and mineralocorticoid synthesis; partial deficiency as observed in congenital adrenal hyperplasia can also redirect precursors into androgen biosynthesis, further aggravating hyperandrogenemia [10,11]. First-line pharmacological treatments for PCOS, such as combined oral contraceptives (COCs) and metformin, reduce androgen levels indirectly [10,12,13]. COCs suppress gonadotropin release, lowering ovarian androgen production, while metformin improves insulin sensitivity, reducing hyperinsulinemia-driven androgen excess. However, these therapies are symptomatic, not curative, and are often associated with side effects such as abnormal uterine bleeding, thromboembolism, and gastrointestinal disturbances. Moreover, androgen levels often rebound after treatment discontinuation [14].

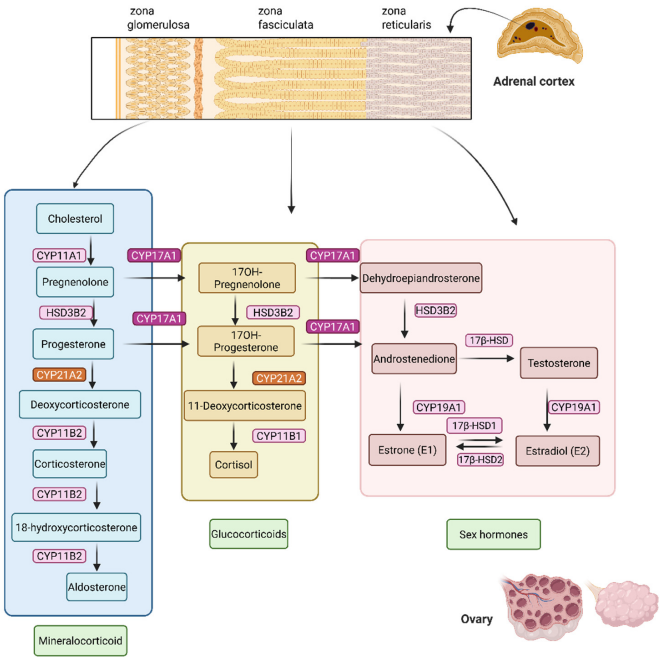


Figure 1. Steroid hormone biosynthesis in the ovary and adrenal cortex. Cholesterol serves as the precursor for all steroid hormones, undergoing enzymatic conversion through distinct pathways in the zona glomerulosa, zona fasciculata, and zona reticularis of the adrenal cortex, as well as in the ovary. Mineralocorticoid pathway (blue box) in the zona glomerulosa leads to aldosterone synthesis via the sequential action of CYP11A1, HSD3B2, CYP21A2, and CYP11B2. Glucocorticoid pathway (yellow box) in the zona fasciculata synthesizes cortisol through the enzymes CYP17A1, HSD3B2, CYP21A2, and CYP11B1. Specifically, CYP17A1 acts on pregnenolone or progesterone to add a 17α-hydroxyl group, producing 17α-hydroxypregnenolone or 17-hydroxyprogesterone, respectively. HSD3B2 converts 17α-hydroxypregnenolone to 17-hydroxyprogesterone (and pregnenolone to progesterone). CYP21A2 converts 17-hydroxyprogesterone to 11-deoxycortisol. CYP11B1 converts 11-deoxycortisol to cortisol. In the zona reticularis and ovarian theca/granulosa cells (pink box), androgens and estrogens are synthesized. CYP17A1 performs both 17α-hydroxylase and 17,20-lyase activities to produce dehydroepiandrosterone (DHEA) from 17α-hydroxypregnenolone. HSD3B2 converts DHEA to androstenedione, 17β-HSD converts androstenedione to testosterone. CYP19A1 (aromatase) converts androstenedione and testosterone into estrogens, such as estrone and estradiol. Enzyme names are shown in boxes next to each reaction step, with pathway products grouped by hormone class (mineralocorticoids, glucocorticoids, sex hormones).

Direct CYP17A1 inhibition offers a more targeted approach to reducing androgen biosynthesis but the dual functionality of CYP17A1 presents a formidable therapeutic challenge [15–20]. Direct inhibition of CYP17A1 is a validated strategy for androgen sup-

pression, exemplified by the drug abiraterone, which is used to treat castration-resistant prostate cancer [21]. However, abiraterone is a non-selective, "blunt instrument" inhibitor, potently blocking both the lyase and the essential hydroxylase activities of CYP17A1 [22,23] as well as inhibiting CYP21A2 [24,25]. This blockade of cortisol synthesis triggers a compensatory surge in adrenocorticotropic hormone (ACTH), leading to an accumulation of mineralocorticoid precursors and a subsequent syndrome of mineralocorticoid excess, characterized by hypertension, hypokalemia, and fluid retention. Consequently, abiraterone therapy necessitates co-administration with exogenous glucocorticoids to prevent adrenal insufficiency, a strategy that carries its own risks and is poorly suited for the long-term management of chronic, non-malignant conditions like PCOS and congenital adrenal hyperplasia. These limitations highlight the need for selective 17,20-lyase inhibitors that suppress androgens while sparing cortisol and mineralocorticoid production [26,27].

The search for novel chemical scaffolds capable of this precise selectivity has led to the investigation of natural products, a historically rich source of unique molecular architectures [28–39]. The root of *Salvia miltiorrhiza* (SM) (Danshen), a staple of traditional Chinese medicine, contains a class of bioactive diterpenoid quinones known as tanshinones [40–44]. These compounds, including tanshinone I (TAI), tanshinone IIA (TAII), and dihydrotanshinone 1 (DT), have demonstrated a wide range of pharmacological activities, and preliminary studies have suggested they may possess endocrine-modulating properties, making them compelling candidates for investigation as steroidogenesis inhibitors [44–50]. Their favorable tolerability profile compared to conventional pharmaceuticals positions them as promising candidates for long-term hormonal modulation [51,52].

This study was therefore designed to systematically investigate the inhibitory effects of a crude *SM* extract and its purified tanshinone constituents on the dual enzymatic activities of CYP17A1. By quantifying their impact on both 17α-hydroxylase and 17,20-lyase functions, as well as on the primary off-target steroidogenic enzyme CYP21A2, we aimed to determine their potential and selectivity as natural product-derived leads for the development of a new generation of safer, more effective therapies for hyperandrogenism.

2. Materials and Methods

2.1. Reagents and Materials

Dried roots of SM were purchased from Inner Mongolia Leihetang Company, Ordos, China. The material was naturally dried at room temperature, ground into a powder, and extracted with analytical-grade acetone. The powder (5 g) was soaked in acetone (100 mL) in an amber glass container and stored in the dark at room temperature for 24 h with intermittent shaking. The mixture was then filtered through filter paper. The residue was re-extracted once under the same conditions, and the filtrates were combined. The solvent was removed by passive evaporation (5–7 days) in a fume hood until the crude extract was dry. The extract was weighed to determine the extraction yield and stored in sealed amber vials at 4 °C (short-term) or −20 °C (long-term).

Abiraterone acetate was acquired from MedChemExpress through Lucerna Chem AG, (Lucerne, Switzerland). Purified tanshinone 1 (CAS# 568-73-0), tanshinone 11A (CAS# 568-72-9) and dihydrotanshinone 1 (CAS# 87205-99-0) were obtained from MedChemExpress (Monmouth Junction, NJ, USA). Radiolabeled substrates progesterone [4-^{14}C] (specific activity: 55 mCi/mmol; concentration: 0.1 mCi/mL), and 17α-hydroxypregnenolone [21-^{3}H] (specific activity: 15 Ci/mmol; concentration: 1 mCi/mL), were purchased from American Radiolabeled Chemicals Inc., (St. Louis, MO, USA). Non-radioactive compounds such as pregnenolone, progesterone, 17α-hydroxy pregnenolone, resazurin sodium salt, and dimethyl sulfoxide (DMSO) were procured from Sigma-Aldrich, St. Louis, MO, USA. Organic solvents were obtained from Carl Roth® GmbH+ Co. KG, Karlsruhe, Germany,

and activated charcoal from Merck AG, Darmstadt, Germany. Silica gel-coated aluminum-backed TLC plates were purchased from Macherey-Nagel, Oensingen, Switzerland. Tritium screens for autoradiography were provided by Fujifilm, Dielsdorf, Switzerland.

2.2. Cell Cultures

Human adrenocortical NCI-H295R cells (ATCC: CRL-2128) were purchased from ATCC and cultured in DMEM/Ham's F-12 medium with L-glutamine and 15 mM HEPES (Thermo Fisher Scientific, Waltham, MA, USA), supplemented with 5% NU-Serum (Becton Dickinson, Franklin Lakes, NJ, USA), 0.1% insulin, transferrin, selenium (100 U/mL; Thermo Fisher Scientific, Waltham, MA, USA), and 1% penicillin (100 U/mL; Thermo Fisher Scientific, Waltham, MA, USA), and streptomycin (100 µg/mL; GIBCO, New York, NY, USA). RWPE-1 cells (ATCC: CRL-36O7) were cultured in keratinocyte serum-free media (K-SFM) supplemented with 0.05 mg/mL bovine pituitary extract and 5 ng/mL epidermal growth factor, and 1% penicillin (100 U/mL; Thermo Fisher Scientific, Waltham, MA, USA), and streptomycin (100 µg/mL; GIBCO). HEK-293T (ATCC: CRL-3216) cells were cultured in DMEM medium with L-glutamine and 15 mM HEPES-NaOH (Thermo Fisher Scientific, Waltham, MA, USA), supplemented with 10% fetal bovine serum (Thermo Fisher Scientific, Waltham, MA, USA), and 1% penicillin (100 U/mL; Thermo Fisher Scientific, Waltham, MA, USA), and streptomycin (100 µg/mL; GIBCO). Passage numbers remained below 30 as per standard procedures. All cell lines were validated and characterized before use to ensure their authenticity and reliability. Routine mycoplasma testing was conducted to confirm that the cells were free from contamination. Additionally, key functional and morphological characteristics were assessed to verify their alignment with previously reported profiles.

2.3. Alamar Blue Assay

The alamarBlue® assay (Thermo Fisher Scientific, Waltham, MA USA) was conducted as previously described [15]. RWPE-1 cells, HEK-293 cells, and NCI-H295R cells were plated in 96-well plates at 10,000 cells per well and incubated overnight at 37 °C with 5% CO_2. After 24 h, the medium was replaced with fresh medium containing the SM at a final concentration between 10–0.01 µg/mL and the pure chemicals from SM (TAI, TAII, and DT) at a final concentration between 10–0.01 µM. Cells were incubated for an additional 24 h. Cell viability was measured using the alamarBlue® assay. Post-incubation, 0.05 mg/mL alamarBlue® solution in phosphate-buffered saline (PBS) was added to each well. The plates were incubated in the dark at 37 °C with 5% CO_2 for 4 h, and fluorescence was measured at an excitation wavelength of 540 nm and an emission wavelength of 590 nm. Cell viability was calculated relative to the control sample treated with DMSO. All experiments were conducted in triplicate [28,29].

2.4. CYP17A1 Assays

Assay of CYP17A1 17α-hydroxylase and 17,20-lyase activities were performed as described previously [15,25,53]. The 17α-hydroxylase activity was measured by conversion of progesterone to 17OH-progesterone, while production of DHEA from 17OH-pregnenolone was used for monitoring the 17,20-lyase activity of CYP17A1. In vitro CYP17A1 assays were performed using a liposome system consisting of human p450 oxidoreductase (POR) and CYP17A1 at a ratio of 3:4 (POR: CYP17A1). The final assay mixture consisted of proteins (37.5 nmol POR: 50 nmol CYP17A1), 10 mM $MgCl_2$, 6 mM potassium acetate (KOAc), 0.05 mg/mL DLPC,1 mM reduced Glutathione in 50 mM HEPES-NaOH buffer (pH 7.4), and the reaction volume was 200 µL. The drugs were added to the final mixture and incubated for 1h before the catalytic reaction was initiated by the addition of NADPH to 1 mM final concentration. Radiolabeled [^{14}C]-progesterone (10,000 cpm in 1 µM) was used as a tracer in each reaction. Steroids were extracted and separated by thin-layer chro-

matography (TLC) on silica gel (SIL G/UV254) TLC plates (Macherey-Nagel, Oensingen, Switzerland) as previously described [15,28].

In vitro CYP17A1 17,20-lyase activity assays were performed using POR, CYP17A1 and cytochrome b_5 as described previously [15]. The final assay mixture consisted of proteins, 10 mM $MgCl_2$, 6 mM KOAc, 0.05 mg/mL DLPC, 1 mM reduced glutathione in 50 mM HEPES-NaOH buffer (pH 7.4), and the reaction volume was 200 µL. The drugs were added to the final mixture and incubated for 1h before the catalytic reaction was initiated by the addition of NADPH to 1 mM final concentration. Radiolabeled [^{3}H]-17OH-pregnenolone (50,000 cpm in 1 µM) was added as a tracer and the enzyme activity was measured by using the scintillation counter in the water release assay [28,29].

2.5. CYP21A2 Assays

Transient transfections were performed using the CYP21A2 WT vector as described previously [54]. HEK293 cells were seeded in six-well plates (3×10^5 cells/well). After 24 h, the growth medium was replaced, and cells were transfected using Lipofectamine 2000 (Thermo Fisher Scientific, Bedford, MA, USA) with 12.5 µg of plasmid (plasmid concentration: 1068 µg/mL). Twenty-four hours after transfection, transfected cells were replated in 24-well plates (1.5×10^5 cells/well) to ensure homogeneity of the cell population across the wells. Six hours after transfection, 2 mL of fresh medium was replaced, and the cells were cultured for 48 h. Cell growth was examined. If cells were growing well, SM, TAI, TAII, and DT were added at a concentration of 10 µg/mL for SM and 10 µM for TAI, TAII, and DT. DMSO was added to the negative control, and 10 µM abiraterone was added to the positive control, and the cells were incubated for 4 h. Functional assays were initiated by adding 1 µM unlabeled progesterone (using 10,000 cpm of [^{14}C]-progesterone as a tracer). After incubation at 37 °C for 1 h, the culture medium and cells were harvested. Steroids were extracted from the culture medium with ethyl acetate and isooctane (1:1 volume ratio), dried, and dissolved in dichloromethane. Steroids were separated by thin-layer chromatography (TLC), placed on a phosphor screen, and visualized using a Typhoon PhosphorImager FLA-7000 (GE Healthcare Bio-Sciences AB, Uppsala, Sweden). Image intensity was measured and quantified using ImageQuant TL v8 (Cytiva, Marlborough, MA, USA). The CYP21A2 enzyme activity was expressed as relative steroid conversion. Steroids were quantified as a percentage of radioactivity incorporated into 11-deoxyprogesterone to the total radioactivity measured in the whole sample and compared between the WT and variants. Cells were collected with trypsin and washed with 1× PBS to quantify the amount of protein. Results were analyzed from three technical replicates. To ensure a similar amount of CYP21A2 in each reaction, a Western blot analysis was performed to normalize the enzyme activity with the relative CYP21A2 expression.

2.6. Western Blot

CYP21A2 expression was determined from total protein extracts. Cells were incubated with the previously described lysis buffer for 1 h and centrifuged at 10,000× *g* for 10 min at 4 °C [54]. The supernatant was collected, and total protein was determined using the Pierce Coomassie Plus (Bradford) assay kit (Thermo Fisher Scientific, Hanover Park, IL, USA). 50 µg of total protein was loaded onto an SDS-PAGE gel (GenScript, Piscataway, NJ, USA) and then transferred to a PVDF membrane as previously described. Two primary antibodies were used: a mouse DKY-Tag monoclonal antibody (GenScript, Catalog No. A00187) at a dilution of 1:1000 and a mouse anti-β-actin monoclonal antibody (Sigma Aldrich, St. Louis, MO, USA, Catalog No. SAB3500350) at a dilution of 1:1500. The secondary antibody, IRDye 800CW-conjugated donkey anti-mouse antibody (LI-COR, Lincoln, NE, USA, Catalog No.

926-32212), was used at a dilution of 1:15,000. Fluorescence signals were detected using an Odyssey SA infrared imaging system (LI-COR Bioscience Inc., Lincoln, NE, USA).

2.7. Computational Details

All calculations were done with the Schrödinger software system (Schrödinger Release 2025-2, Schrödinger, LLC, New York, NY, USA, 2025). Structures of the tanshinones were extracted from the PubChem database and subjected to the Ligand Preparation procedure in Maestro (v. 14.4.133) prior to the docking studies [55,56]. Protein structures were extracted from the Protein Data Bank and subjected to the Protein Preparation Procedure in Maestro [55,57]. Only the A-chain was used except for the 5IRQ structure, where both the A- and C-chains were used, since they contained different enantiomers of the ligand, *(R)*- and *(S)*-orteronel, respectively [58]. The GLIDE docking program (v2025-2 build 133) was used for the docking studies using the default setup. Receptor Grid Generation was defined by the ligand present in the CYP17A1 active site. The standard precision (SP) mode for scoring the poses was applied. For each compound up to 100 poses were collected and further refined by the default post-docking minimization available in GLIDE. The ten best scoring poses were visually inspected and subjected to MM-GBSA (Molecular Mechanics/Generalized Born Surface Area) energy calculation. The binding modes were described by a combination of the subjective terms "down/up" and "left/right" with reference to the orientation of the furane oxygen atom relative to the heme group. The MM-GBSA energy calculations were done with the Prime module (v2025-2 build 133) in Maestro. This method calculates both the free energy of binding and the individual energy contributions to the free energy. One representative of each binding mode of each compound was selected for molecular dynamics (MD) simulation. The MD simulations were performed with the Desmond program (v8.2.133) and comprised a default seven step equilibration procedure followed by a 50 ns production run at 300 K using the OPLS4 force field. For each simulation 50 frames were collected and analyzed. Structures were displayed with the Pymol program (v.3.1.5.1).

2.8. Data Analysis

Data analysis was conducted using RStudio (version 3.6.0+) and GraphPad Prism (GraphPad Software, Inc., San Diego, CA, USA) to ensure a thorough evaluation. Results are expressed as the mean ± standard deviation (SD) from three independent experiments to account for variability and reproducibility. One-way analysis of variance (ANOVA) was used to evaluate differences between treatment groups and controls, with post hoc analyses performed using Tukey's Honest Significant Difference (HSD) test to identify specific differences. Significance was determined with thresholds of * $p < 0.05$ and ** $p < 0.001$. All tests were two-tailed, and assumptions of normality and variance homogeneity were checked prior to analysis to validate the ANOVA results.

3. Results

3.1. Computational Strategy

Molecular docking and binding energy calculations of the ligands tanshinone IIA, dihydrotanshinone I, and tanshinone I (Figure 2) were employed to evaluate the potential binding affinity and orientation of selected tanshinone derivatives within the active site of human CYP17A1.

The computational workflow was designed to provide a comprehensive in silico assessment, moving from initial, broad-spectrum docking to more refined and energetically rigorous calculations. This process involved an exhaustive screen of all available CYP17A1 crystal structures to identify the most suitable model for a more detailed analysis. The

A105L mutant bound to 17α-hydroxypregnenolone (PDB: 4NKZ, chain A) was selected for the subsequent docking studies due to its favorable and representative active site conformation for the compounds under investigation.



Figure 2. Structure of pure SM components tanshinone I, tanshinone IIa and dihydrotanshinone I.

The final refinement of binding energy estimates was performed using MM-GBSA (Molecular Mechanics/Generalized Born Surface Area) calculations, a method that provides a more discriminative assessment of binding free energy by accounting for solvation effects and conformational entropy, which are often overlooked in simpler docking scores. MD simulations were performed on selected binding poses to explore the stability of the protein-ligand complex and flexibility of the ligand.

3.2. Molecular Docking and Binding Energy Analysis

Initially we performed a GLIDE based docking of the three tanshinones in all the human CYP17A1 structures available in the Protein Data Bank (Figure 3).



Figure 3. Heatmap showing the GLIDE docking scores for docking of the three tanshinones in the human CYP17A1 structures. Only the A-chain was used, except for 5IRQ, where both the A- and C-chains were used, since they contained different enantiomers of the ligand, *(R)*- and *(S)*-orteronel, respectively. The right column shows the scale in kcal/mol used in the heatmap.

The docking score varies for the different structures reflecting that the active sites are slightly different in shape and charge distribution. The best scores are obtained for the CYP17A1 structures with the A105L mutation (4NKV, 4NKW, 4NKX, 4NKY and 4NKZ), which induces a minor conformational change in the active site supposed to make the structure more lyase like [59]. The subsequent studies were all done on the 4NKZ structure, as this was associated with the overall best score.

Inspection of the GLIDE poses revealed that there are no significant differences in the binding modes of the three tanshinones. The molecules are essentially planar and bind in four different ways with nearly identical shape. In the following descriptions, we refer to the four binding modes with a combination of the labels "up–down" and "left–right" reflecting their orientation to the heme group (Figures 4 and 5, Table 1).

The "up–right" binding mode, which represents the best scoring pose for dihydrotanshinone I and tanshinone I, is especially interesting, because it is the only binding mode with a direct contact to the protein, a hydrogen-bond to Arg239 (Figure 5).

Docking programs are generally better to predict correct binding modes than binding energies, because the former primarily is controlled by specific interactions like hydrogen-bonding and charge-charge interactions whereas binding energies often depend on more diffuse interactions like non-polar interactions and hydrophobic effects like desolvation and solvation [60].

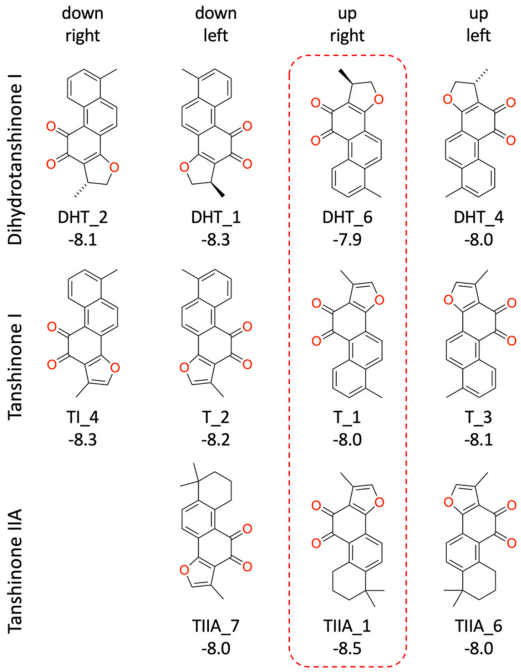


Figure 4. GLIDE binding modes for three tanshinones. The labels below each structure refer to the docking pose and the GLIDE docking score in kcal/mol. For data for all the GLIDE poses see Table 1.

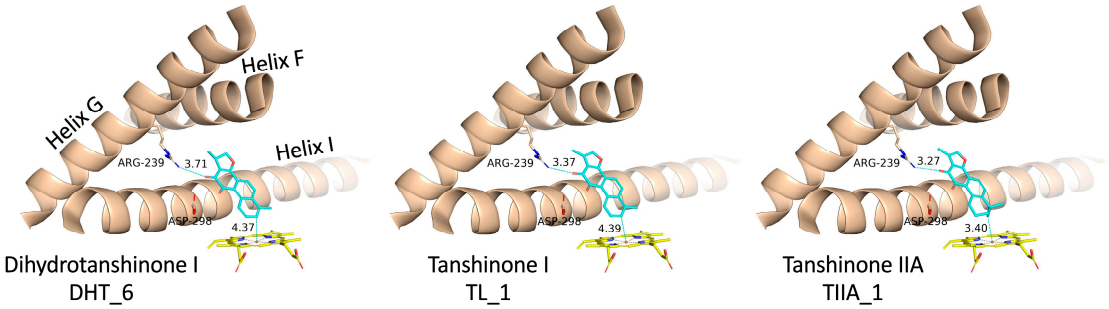


Figure 5. The "up–right" binding mode for the three tanshinones. For CYP17A1 Helix F, G and I are shown as a cartoon, Arg239, Asp298 and the heme group as type-colored stick models. The labels below the ligand names refer to the GLIDE poses (see Figure 4 and Table 1).

In Table 1 we have collected the binding scores/energies for the different binding modes. If we use the approach recommended by Schrodinger, the lowest E model energy corresponds to the preferred binding mode for each ligand, whereas the docking score should be used to compare binding of different ligands (https://my.schrodinger.com/support/article/1027 accessed on 1 October 2025). Nevertheless, the differences in docking scores are too small to be significant and, accordingly, we have subjected the GLIDE poses to a more rigorous energy determination method. The MM-GBSA method is a molecular mechanics-based (MM) method for calculation of binding energies combined with an implicit continuum treatment of solvation by a generalized Born (GB) and solvent area (SA) based approach [61]. The MM-GBSA method is often used for post-evaluation of docking scores to achieve better binding energies [62,63].

MM-GBSA calculations, which estimate the free energy of binding, predicted that TAI (−44.32 kcal/mol) and TAII (−41.73 kcal/mol) were thermodynamically more favorable binders than DT (−40.95 kcal/mol) (Table 1). This is in direct opposition to our experimental data, where DT is the most potent functional inhibitor. This apparent discrepancy is a critical finding, suggesting that static binding affinity alone does not dictate inhibitory efficacy. Instead, the distinct binding pose adopted by DT, though potentially less stable,

appears to be more functionally disruptive to the lyase catalytic cycle. This highlights the limitation of using thermodynamic energy scores as the sole predictor of biological activity and points toward the paramount importance of specific inhibitor–enzyme geometry for functional outcomes [64,65].

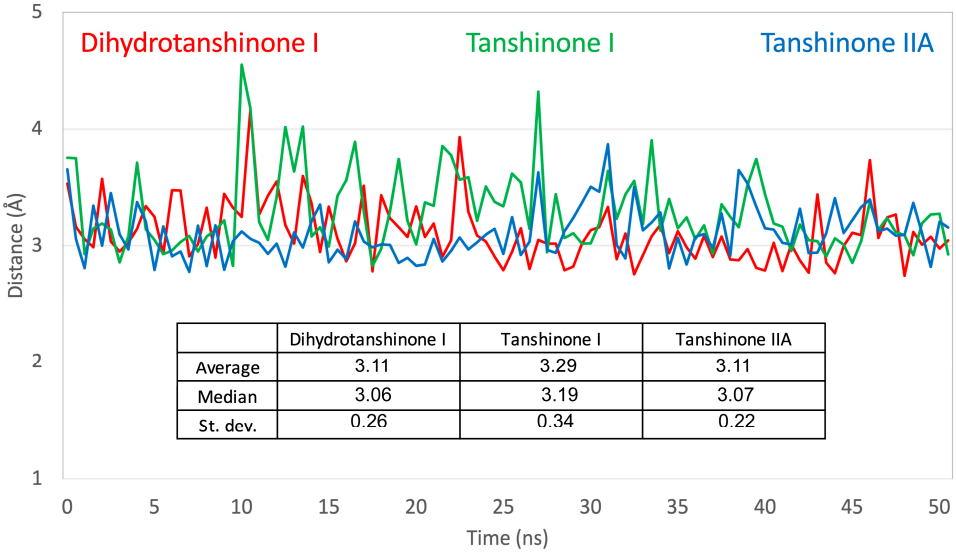
Table 1. Binding energies for the GLIDE docking poses. See text for details on the different energy terms. Binding mode refers to the binding modes described in Figure 4. Each energy column is color coded continuously with lowest energy value green and highest energy value red. Poses in yellow boxes were selected for MD simulations. All energies are kcal/mol.

Compound	Pose	Docking Score	GLIDE Emodel	MMGBSA dG Bind	Binding Mode
Dihydrotanshinone I	1	−8.2	−62.2	−39.5	down–left
	2	−8.1	−62.1	−30.6	down–right
	3	−8.1	−62.2	−41.0	down–left
	4	−8.0	−59.5	−35.2	up–left
	5	−8.0	−60.6	−39.4	down–left
	6	−7.9	−58.5	−39.3	up–right
	7	−7.9	−60.6	−31.5	down–right
	8	−7.8	−59.9	−34.2	up–left
	9	−7.7	−58.4	−39.3	up–right
	10	−6.0	−30.3	−6.7	up–right
Tanshinone I	1	−8.3	−62.7	−44.4	up–right
	2	−8.2	−64.6	−40.8	down–left
	3	−8.1	−61.6	−36.4	up–left
	4	−8.0	−62.6	−40.2	down–right
	5	−8.0	−61.4	−44.4	up–right
	6	−7.9	−58.5	−42.4	down–left
	7	−7.8	−56.7	−39.1	down–left
	8	−7.6	−53.8	−37.9	up–left
	9	−7.0	−50.2	−44.3	up–right
	10	−5.9	−25.7	2.1	skewed
Tanshinone IIA	1	−8.5	−62.1	−34.9	up–right
	2	−8.3	−59.8	−41.6	up–right
	3	−8.2	−59.7	−26.9	up–left
	4	−8.1	−59.8	−41.8	up–right
	5	−8.1	−59.9	−47.1	up–right
	6	−8.0	−58.8	−29.6	up–left
	7	−7.9	−56.7	−31.6	down–left
	8	−7.8	−56.7	−26.2	down–left
	9	−7.8	−57.3	−32.1	up–left
	10	−7.6	−50.9	−20.1	down–left

3.3. Molecular Dynamics Simulations

To further characterize the binding of the tanshinones to CYP17A1 we subjected one representative (with the best docking score) of each of the eleven binding modes shown in Figure 4 to short MD simulations. In all eleven MD simulations the systems were stable and the ligand remained in the active site. Nevertheless, the complexes with the "up–right" binding mode had significantly smaller RMSD values for the protein Ca atoms. The ligands, the tanshinones, also displayed lower RMSD values relative to the protein than

observed for the other binding modes. Thus, we conclude, that the "up–right" binding mode with the hydrogen-bond from Arg239 to one of the ligand carbonyl oxygens has a stabilizing effect on the complexes. The Arg239-ligand hydrogen-bond fluctuate, but we see a preference for a slightly shorter hydrogen bond and a slightly smaller variation for dihydrotanshinone I and tanshinone IIA than for tanshinone I (Figures 6 and 7), suggesting a stronger hydrogen-bond for these two ligands. This interaction is hypothesized to be a critical anchor point that orients the planar tanshinone scaffold within the active site, contributing to the stability and potentially the inhibitory activity of the compounds.



	Dihydrotanshinone I	Tanshinone I	Tanshinone IIA
Average	3.11	3.29	3.11
Median	3.06	3.19	3.07
St. dev.	0.26	0.34	0.22

Figure 6. Variation in the hydrogen bond between Arg239 and tanshinone ligands. Dynamic behavior of the key Arg239-ligand hydrogen bond in the 'up–right' binding pose during 50 ns MD simulations. The plot displays the variation of hydrogen bond distances (in Ångstroms) between the guanidinium group of Arg239 and one of the proximal carbonyl oxygen of each tanshinone ligand. The inset table provides key statistics, including the mean distance and standard deviation.

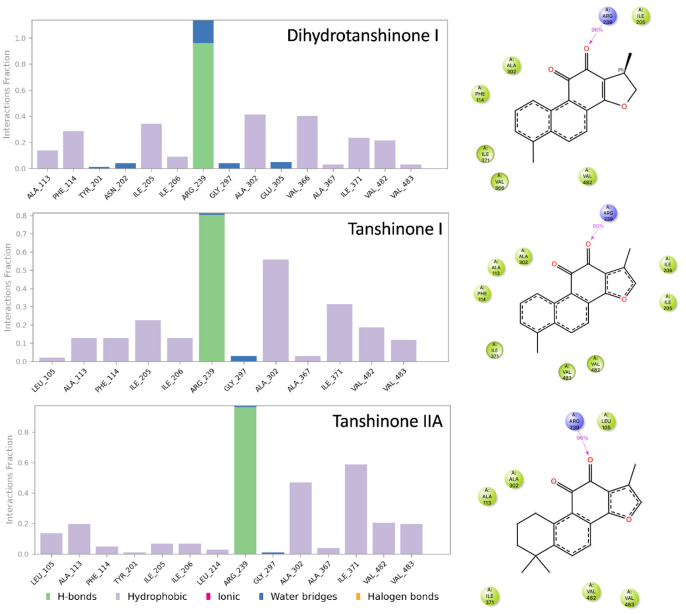


Figure 7. Simulation interaction diagrams. The bar diagrams (**left**) show the interactions between the protein CYP17A1 and the ligands during the MD simulation. Key to type of interactions shown below bar diagrams. The structures (**right**) display the intramolecular interactions present in more than 30% of the frames sampled during the MD simulations. Light green and dark blue symbols refer to hydrophobic and hydrogen-bonding interactions, respectively.

3.4. Cell Lines and Cytotoxicity Assays

3.4.1. Cytotoxicity of Tanshinones in Adrenal, Kidney, and Prostate Cell Lines

To establish a therapeutic window and determine appropriate concentrations for subsequent enzyme inhibition assays, the cytotoxic effects of the SM extract and its purified components were assessed across three distinct human cell lines: NCI-H295R (adrenocortical carcinoma), HEK-293T (embryonic kidney), and RWPE-1 (normal prostate epithelium). As summarized in Table 2 and Figure 8, dihydrotanshinone (DT) exhibited the most consistent cytotoxic effects across all three cell lines, with half-maximal inhibitory concentrations (IC_{50}) ranging from 0.95 μM to 1.40 μM. The other pure compounds, TAI and TAII, also induced cell death in the low single-digit micromolar range. However, the data for TAI and TAII showed greater variability between cell lines and larger experimental variance, particularly in the RWPE-1 cell line (e.g., TAII IC_{50} 4.50 μM), which precludes a precise comparative ranking of their potency. The crude SM extract was cytotoxic in the low μg/mL range, with the highest potency observed in the RWPE-1 cell line (IC_{50} 1.12 μg/mL). Based on these findings, a non-toxic concentration of 10 μM for the pure compounds and 10 μg/mL for the SM extract was selected for all subsequent enzyme activity assays.

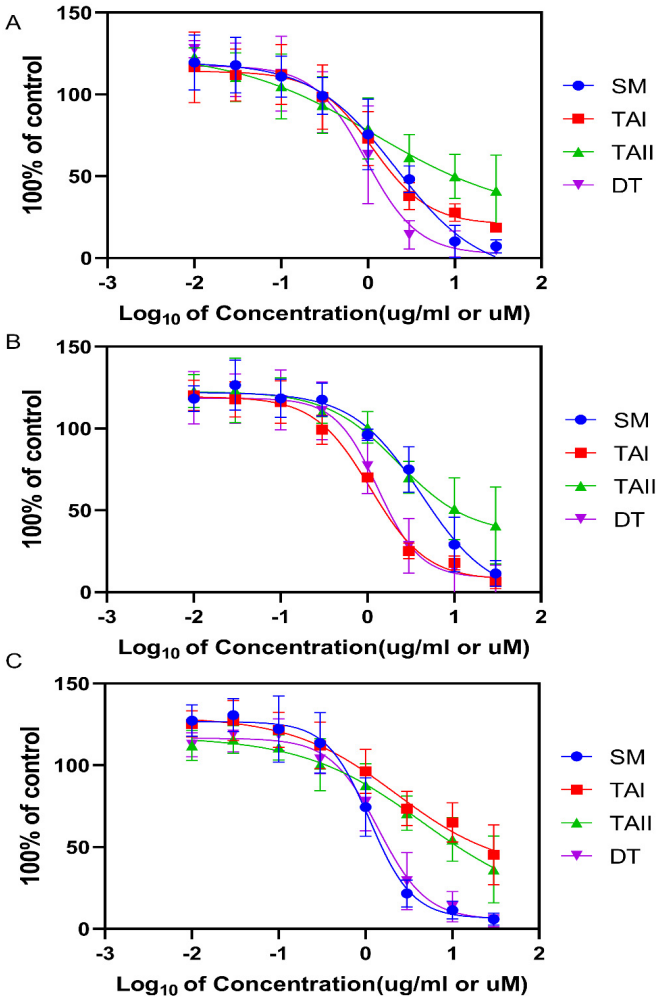


Figure 8. Cytotoxicity of *SM* extract and purified tanshinones in human cell lines. Dose–response curves show the effect of increasing concentrations of SM extract (μg/mL), TAI (μM), TAII (μM), and DT (μM) on the viability of (**A**) NCI-H295R adrenocortical, (**B**) HEK-293T kidney, and (**C**) RWPE-1 prostate epithelial cells after 24-h incubation. Cell viability was determined using the alamarBlue® assay and is expressed as a percentage of the vehicle (DMSO) control. Data points represent the mean ± SD of three independent experiments. The IC_{50} values derived from these curves are summarized in Table 2.

Table 2. Cytotoxicity (IC_{50}) of SM extract and purified tanshinones in human cell lines. Values are presented as mean ± standard deviation from three independent experiments.

Drug	NCI-H295R (IC_{50})	HEK-293T (IC_{50})	RWPE-1 (IC_{50})
SM	2.11 ± 1.80 μg/mL	4.17 ± 2.56 μg/mL	1.12 ± 0.31 μg/mL
TAI	1.13 ± 0.63 μM	1.08 ± 0.26 μM	2.27 ± 3.25 μM
TAII	1.20 ± 3.44 μM	2.26 ± 1.92 μM	4.50 ± 11.80 μM
DT	0.95 ± 0.48 μM	1.31 ± 0.47 μM	1.40 ± 0.42 μM

3.4.2. In Silico Assessment of Physicochemical Properties and Pharmacokinetic Profile

To build a more comprehensive preclinical profile and anticipate potential developmental challenges, a thorough in silico analysis of the absorption, distribution, metabolism, and excretion (ADME) properties of the lead tanshinones was performed using the SwissADME toolkit [66]. We compared the properties of tanshinone I (TAI), tanshinone IIA (TAII), and the most potent and selective inhibitor, dihydrotanshinone I (DT). The analysis of fundamental physicochemical properties reveals that all three compounds are well within the ranges defined by established oral drug-likeness filters (Table 3). All compounds possess molecular weights under 300 g/mol, a favorable consensus Log P (lipophilicity) between 3.0 and 3.8, and, critically, zero violations of Lipinski's Rule of Five, suggesting a high potential for oral bioavailability. A notable distinction emerged in the overall bioavailability score, a composite metric that integrates multiple physicochemical parameters. DT is predicted to have a superior bioavailability score of 0.85, compared to 0.55 for both TAI and TAII. This advantage for DT appears to be driven by its slightly lower lipophilicity (Consensus Log P = 3.03) and significantly higher predicted aqueous solubility (ESOL Class: Soluble) relative to the other two analogs. This predicted enhancement in oral bioavailability represents a significant advantage, as it can directly translate to improved dosing regimens, better therapeutic efficacy, and enhanced patient compliance, further strengthening the rationale for prioritizing DT as the lead scaffold.

Predicted pharmacokinetic behaviors indicate that all three compounds are likely to exhibit high gastrointestinal (GI) absorption and are capable of permeating the blood–brain barrier (BBB). While high GI absorption is desirable, the predicted BBB permeability raises the possibility of central nervous system (CNS) exposure, which could lead to off-target neurological effects. This is a critical parameter that would require careful monitoring in subsequent in vivo preclinical safety studies. A key predicted differentiator was found in their interaction with the P-glycoprotein (P-gp) efflux pump, a major mechanism of drug resistance. While TAI and DT are not predicted to be P-gp substrates, TAII is, which could limit its effective intracellular and tissue concentrations and potentially compromise its efficacy.

The in silico models predict that the tanshinone scaffold may inhibit other CYP isoforms. All three compounds are predicted to be inhibitors of CYP1A2 and CYP2C19. Furthermore, TAII and DT are also predicted to inhibit CYP2C9, CYP2D6, and CYP3A4. This predicted broad-spectrum CYP inhibition represents a major developmental red flag. The five enzymes predicted to be inhibited by DT (CYP1A2, CYP2C19, CYP2C9, CYP2D6, and CYP3A4) are collectively responsible for the metabolism of over 90% of all clinically prescribed drugs. The target patient populations for a CYP17A1-lyase inhibitor, such as individuals with PCOS or congenital adrenal hyperplasia, frequently have comorbidities and are often on multiple medications (e.g., metformin, oral contraceptives, statins, glucocorticoids), many of which are substrates for these CYP enzymes. Co-administration of a potent CYP inhibitor like DT could elevate the plasma concentrations of these concomitant medications, leading to toxicity. Finally, structural analysis using medicinal chemistry filters identified potential intrinsic liabilities. All three compounds registered two PAINS

(Pan-Assay Interference Compounds) alerts, specifically for the "imine_one_A_quinone_D" substructure, and one Brenk alert for a "diketo_group". These alerts flag chemical motifs that are known to be potentially reactive, prone to non-specific binding, and can interfere with assay readouts. The presence of these reactive moieties may mechanistically underlie not only the observed cytotoxicity but also some of the predicted toxicity endpoints.

Table 3. Comparative in Silico ADME and physicochemical profile of tanshinones from SwissADME predictions.

Parameter	Tanshinone I (TAI)	Tanshinone IIA (TAII)	Dihydrotanshinone I (DT)
Formula	$C_{18}H_{12}O_3$	$C_{19}H_{18}O_3$	$C_{18}H_{14}O_3$
MW (g/mol)	276.29	294.34	278.30
Consensus Log P	3.40	3.80	3.03
TPSA (Å^2)	47.28	47.28	43.37
ESOL Solubility Class	Moderately soluble	Moderately soluble	Soluble
GI Absorption	High	High	High
BBB Permeant	Yes	Yes	Yes
P-gp Substrate	No	Yes	No
CYP1A2 Inhibitor	Yes	Yes	Yes
CYP2C19 Inhibitor	Yes	Yes	Yes
CYP2C9 Inhibitor	No	Yes	Yes
CYP2D6 Inhibitor	No	Yes	Yes
CYP3A4 Inhibitor	Yes	Yes	Yes
Bioavailability Score	0.55	0.55	0.85
Lipinski Violations	0	0	0
PAINS Alerts	2	2	2

3.4.3. Predictive Toxicological Assessment

To identify potential safety liabilities and guide future optimization efforts, a comprehensive in silico toxicological assessment was conducted using the ProTox-3.0 server (Table 4) [67]. At the organ level, the predictions were generally favorable for several critical systems. None of the three tanshinones were predicted to be hepatotoxic, neurotoxic, nephrotoxic, or cardiotoxic. However, all three compounds were predicted to be active for respiratory toxicity, with moderate-confidence probabilities ranging from 0.56 for TAII to 0.66 for DT. More significant toxicological flags were raised for systemic toxicity endpoints, where clear differences between the analogs emerged. While TAI and TAII were predicted to be inactive, DT was predicted to be carcinogenic with borderline confidence (Prob. 0.50). More alarmingly, DT was also predicted to be immunotoxic with very high confidence (Prob. 0.98). This high-probability prediction for immunotoxicity is a concerning finding from the in silico safety assessment. Immunotoxicity can manifest as either immunosuppression or inappropriate immune activation (hypersensitivity), and it is a frequent cause of attrition for drug candidates in later stages of development. The exceptionally high confidence score of 0.98 suggests that the predictive model identified strong structural precedents for this liability within its training data. A plausible mechanistic basis for this prediction can be formed by linking it to the structural alerts identified previously. The quinone-type substructure flagged by the PAINS analysis is a known structural class of haptens, small, reactive molecules that can covalently bind to endogenous proteins. This

creates neoantigens that are subsequently recognized as foreign by the immune system, triggering a drug-specific immune response.

Table 4. Summary of key in silico toxicity predictions for tanshinones from ProTox-3.0 predictions. "Active" predictions are highlighted in bold.

Toxicity Endpoint	Tanshinone I (TAI)	Tanshinone IIA (TAII)	Dihydrotanshinone I (DT)
Hepatotoxicity	Inactive (0.63)	Inactive (0.71)	Inactive (0.62)
Respiratory Toxicity	**Active (0.63)**	**Active (0.56)**	**Active (0.66)**
Carcinogenicity	Inactive (0.51)	Inactive (0.56)	**Active (0.50)**
Immunotoxicity	Inactive (0.66)	Inactive (0.80)	**Active (0.98)**
Mutagenicity	Inactive (0.55)	Inactive (0.70)	Inactive (0.55)
GABA Receptor Activity	**Active (0.51)**	**Active (0.59)**	**Active (0.50)**
AChE Inhibition	Inactive (0.87)	Inactive (0.77)	**Active (0.79)**
PXR Activation	Inactive (0.59)	**Active (0.58)**	**Active (0.58)**

Analysis of molecular-level interactions provided further mechanistic hypotheses for potential off-target effects. All three compounds were predicted to be active at the GABA receptor, and DT was additionally predicted to inhibit acetylcholinesterase (AChE), suggesting potential for neurological side effects. A particularly complex interaction was predicted with the Pregnane X Receptor (PXR), a key nuclear receptor that governs the transcriptional regulation of many drug-metabolizing enzymes and transporters. Both TAII and DT were predicted to be PXR activators. This creates a complicated regulatory scenario when viewed in conjunction with the ADME predictions. PXR activation leads to the transcriptional induction of the *CYP3A4* gene, increasing the synthesis of CYP3A4 protein. However, the SwissADME data (Table 3) concurrently predicts that these same compounds act as direct inhibitors of CYP3A4 activity. This dual activity, enzyme induction at the genetic level and direct inhibition at the protein level, can lead to highly complex and unpredictable drug–drug interaction profiles in vivo. The net effect could change over time, with initial inhibition of drug metabolism potentially followed by a return to normal or even accelerated metabolism as more enzyme is produced. This complex interaction profile further elevates the DDI risk and reinforces the conclusion that the tanshinone scaffold requires significant medicinal chemistry optimization to be clinically viable.

3.5. Tanshinones Selectively Inhibit CYP17A1 17,20-Lyase Activity While Sparing 17α-Hydroxylase Activity

The primary objective was to assess the ability of tanshinones to selectively inhibit the androgen-producing 17,20-lyase function of CYP17A1 while sparing its 17α-hydroxylase function. In a reconstituted microsomal system, none of the tested tanshinones or the SM extract significantly inhibited 17α-hydroxylase activity at concentrations of 10 μM or 10 μg/mL, respectively. Residual hydroxylase activity remained above 93% for all natural compounds, in stark contrast to the non-selective inhibitor abiraterone, which ablated this activity to just 5.3% of the control (Figure 9A).

These data provide the first line of evidence for the preferential inhibition of the lyase reaction by the tanshinone scaffold. Conversely, the compounds demonstrated clear inhibitory effects on 17,20-lyase activity (Figure 9B). Dihydrotanshinone (DT) emerged as the most potent inhibitor among the natural compounds, reducing lyase activity to 43% of the control. The crude SM extract also showed significant inhibition (61% residual activity),

followed by TAII (57%) and TAI (72%). Abiraterone, as expected, was the most potent inhibitor overall, with a residual activity of 30%.

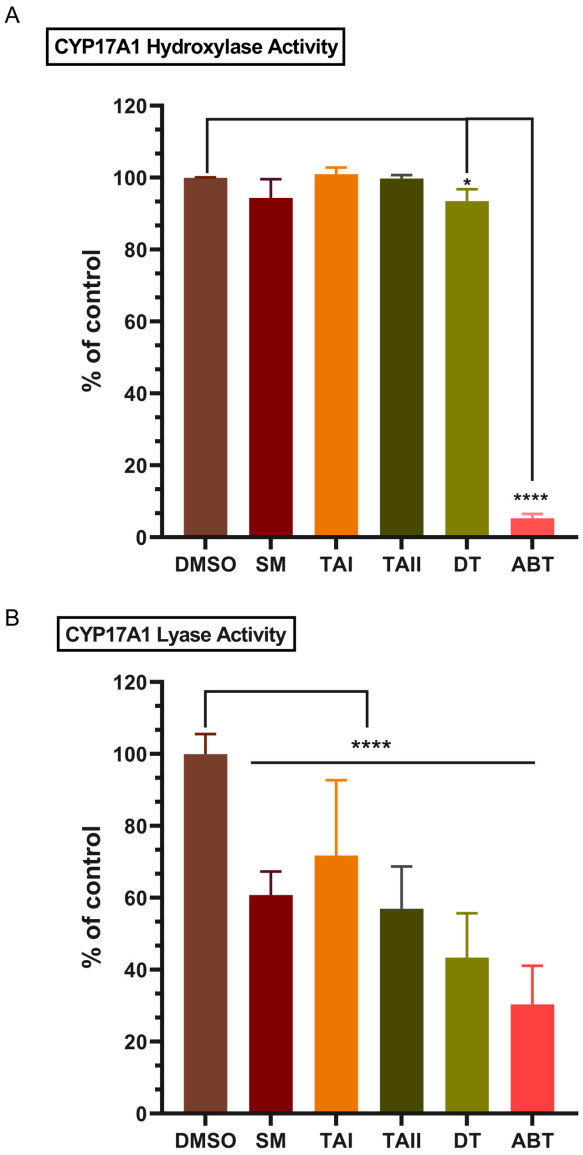


Figure 9. Selective inhibition of CYP17A1 17,20-lyase activity by tanshinones. The residual enzymatic activity of (**A**) CYP17A1 17α-hydroxylase and (**B**) CYP17A1 17,20-lyase following incubation with vehicle (DMSO), abiraterone (ABT, 10 μM), *Salvia miltiorrhiza* extract (SM, 10 μg/mL), TAI (10 μM), TAII (10 μM), and DT (10 μM). Activities were measured in a reconstituted microsomal system and are expressed as a percentage of the DMSO control. Data represent the mean ± SD from three independent experiments. Statistical significance was determined by one-way ANOVA with Tukey's post hoc test. * $p < 0.05$, **** $p < 0.001$. The data demonstrates that DT and SM selectively inhibit the lyase reaction while sparing the hydroxylase function, unlike the non-selective inhibitor abiraterone.

3.6. Tanshinones Exhibit a Favorable Safety Profile with Minimal Inhibition of CYP21A2

A critical liability of non-selective CYP17A1 inhibitors like abiraterone is the concurrent inhibition of CYP21A2 (21-hydroxylase), an enzyme essential for cortisol and aldosterone synthesis. Such off-target inhibition disrupts the glucocorticoid pathway, leading to clinically significant side effects. To assess the potential for this liability, the inhibitory effects of the compounds on CYP21A2 activity were evaluated in HEK-293T cells transiently expressing the enzyme. A critical liability of abiraterone is its off-target inhibition of CYP21A2. When tested in a cell-based assay, the SM extract, TAI, and TAII

showed no meaningful inhibition of CYP21A2. DT exhibited only modest inhibition (85% residual activity), a profile that contrasts sharply with abiraterone, which significantly reduced CYP21A2 activity to 70% of the control (Figure 10). To quantify the degree of selectivity, we calculated selectivity indices based on the observed inhibition percentages (Table 5). This analysis revealed that DT possesses an 8.67-fold selectivity for the lyase over the hydroxylase reaction, a stark contrast to the non-selective profile of abiraterone (index = 0.73). Furthermore, DT demonstrated a favorable therapeutic index against the primary off-target, inhibiting the lyase reaction 3.8-fold more potently than CYP21A2. This finding suggests that tanshinone-based inhibitors may avoid the downstream metabolic consequences that complicate abiraterone therapy.

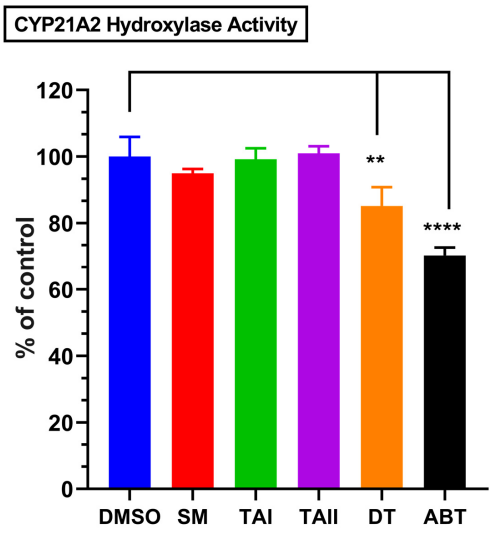


Figure 10. Minimal inhibition of off-target CYP21A2 by tanshinones. The bar chart displays the residual enzymatic activity of CYP21A2 following incubation with vehicle (DMSO), abiraterone (ABT, 10 μM), *Salvia miltiorrhiza* extract (SM, 10 μg/mL), TAI (10 μM), TAII (10 μM), and DT (10 μM). Activity was measured in transiently transfected HEK-293T cells and is expressed as a percentage of the DMSO control. Data represent the mean ± SD from three independent experiments. Statistical significance was determined by one-way ANOVA with Tukey's post hoc test. ** $p < 0.01$, **** $p < 0.001$. The results show that DT exhibits only modest inhibition of CYP21A2, while other natural compounds have negligible effects, contrasting with the significant inhibition caused by abiraterone.

Table 5. Summary of enzyme inhibition and calculated selectivity indices. Data are derived from Figures 4 and 5. Inhibition percentages calculated as (100%—% Residual Activity). [a] Calculated as (% Inhibition Lyase)/(% Inhibition OH). [b] Calculated as (% Inhibition Lyase)/(% Inhibition CYP21A2). [c] Selectivity index is mathematically high but therapeutically limited due to low absolute potency against the lyase activity at the tested concentration.

Compound	% Inhibition CYP17A1-Lyase	% Inhibition CYP17A1-OH	% Inhibition CYP21A2	Lyase/OH Selectivity Index [a]	Lyase/CYP21A2 Selectivity Index [b]
SM	39.2%	5.6%	5.0%	6.96	7.82
TAI	28.2%	<1%	<1%	High [c]	High [c]
TAII	43.0%	<1%	<1%	High [c]	High [c]
DT	56.6%	6.5%	14.9%	**8.67**	**3.80**
Abiraterone	69.6%	94.7%	29.8%	**0.73**	**2.34**

3.7. Inhibition of CYP21A2 Is Mediated by Direct Catalytic Interference, Not Altered Protein Expression

To investigate whether the observed effects on CYP21A2 activity were attributable to changes in protein levels, a Western blot analysis was performed on lysates from the

treated HEK-293T cells. Interestingly, the changes in CYP21A2 protein expression did not correlate with the enzymatic activity data (Figure 11). For instance, treatment with DT and TAII led to a slight increase in CYP21A2 protein levels (normalized densitometry values of 1.15 and 1.30, respectively) compared to the DMSO control (1.07). This occurred despite DT causing modest enzymatic inhibition and TAII having no effect on activity.

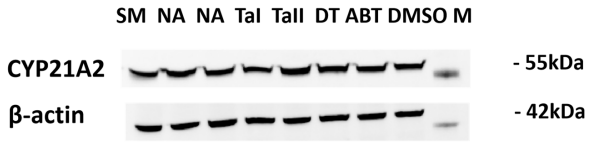


Figure 11. Effect of tanshinones on CYP21A2 Protein Expression. Representative Western blot of CYP21A2 protein levels in transiently transfected HEK-293T cells treated for 4 h with vehicle (DMSO), abiraterone (ABT), SM, TAI, TAII, or DT. β-actin was used as a loading control and densitometric quantification of CYP21A2 protein bands was performed by normalization to β-actin. Data is expressed relative to DMSO control. The results show that the modest inhibition of CYP21A2 activity by DT is not associated with a decrease in protein expression, indicating a direct effect on enzyme catalysis rather than protein stability or synthesis. The original Western blot images in Supplementary Materials also include two extra compounds Marjoram and Chinese dodder (shown as NA), which are not part of the current study and were loaded as part of a larger set.

This discordance suggests that the observed enzymatic inhibition by DT is a direct effect on the catalytic function of the CYP21A2 enzyme itself, rather than a consequence of reduced protein expression. The modest upregulation of CYP21A2 protein in response to some treatments may reflect a secondary cellular feedback or stress response, where the cell attempts to compensate for perceived pathway disruption by increasing enzyme synthesis. This rules out transcriptional or translational downregulation as the primary mechanism of action for the observed effects on CYP21A2.

4. Discussion

This study provides compelling evidence that dihydrotanshinone (DT) and the crude extract of SM function as novel, natural product-derived selective inhibitors of the 17,20-lyase activity of CYP17A1. The central finding is that these compounds, particularly DT, potently inhibit the final androgen-producing step in the steroidogenic cascade while demonstrating markedly reduced activity against both the 17α-hydroxylase function of CYP17A1 and the critical off-target enzyme, CYP21A2. This dual selectivity addresses a major challenge in endocrine pharmacology and represents a significant advancement toward a safer therapeutic profile for managing hyperandrogenic disorders like PCOS and certain forms of prostate cancer.

The therapeutic imperative for such selectivity is best understood in the context of the current clinical standard, abiraterone. Abiraterone is a potent and irreversible inhibitor of both CYP17A1 activities. By blocking the 17α-hydroxylase reaction, it shuts down the production of cortisol. The resulting hypocortisolism triggers a compensatory surge in pituitary adrenocorticotropic hormone (ACTH), which in turn overstimulates the upstream steps of the adrenal cascade. This leads to an accumulation of mineralocorticoid precursors and the development of a mineralocorticoid excess syndrome, characterized by hypertension, hypokalemia, and fluid retention. To mitigate these serious side effects, abiraterone must be co-administered with a glucocorticoid like prednisone, which creates its own set of long-term therapeutic burdens. The compounds identified in this study, by sparing both 17α-hydroxylase and CYP21A2, have the potential to uncouple androgen suppression from cortisol disruption. This profile could obviate the need for glucocorticoid

co-therapy, a profound clinical advantage, especially for chronic, non-malignant conditions like congenital adrenal hyperplasia and PCOS where long-term safety is paramount.

The structural basis for this observed selectivity can be rationalized through molecular modeling, although such in silico approaches must be interpreted with caution as hypothesis-generating tools rather than definitive proof [68,69]. Structurally, CYP17A1's dual catalytic functions mediated by separate active sites for hydroxylase and lyase enable the design of selective inhibitors [70]. SM and DT likely bind preferentially to the lyase site or induce conformational changes that selectively impair lyase function without affecting hydroxylase catalysis. This hypothesis is supported by recent structure–function studies and molecular docking analyses. This complexity of conformational changes upon substrate binding or due to interaction with cytochrome b_5, offers multiple avenues through which a small molecule could selectively interfere with only the second catalytic step. The docking models provide a structural hypothesis for the selectivity of DT that can now be tested experimentally through techniques like site-directed mutagenesis.

The primary finding of this study is the potent and selective inhibition of CYP17A1 17,20-lyase activity by DT. DT reduced the lyase activity to 43% of control levels while having negligible effects on 17α-hydroxylase function, which remained above 93% of control. This exceptional selectivity is quantitatively supported by the calculated selectivity index of 8.67 for DT, which dramatically surpasses the index of 0.73 for the non-selective CYP17A1 inhibitor abiraterone. A central mechanistic insight from our study emerges from the apparent paradox between the computational binding energy predictions and the experimental enzyme inhibition data. While MM-GBSA calculations suggested DT was the weakest binder of the three tanshinones, it was experimentally the most potent inhibitor. This is likely not a model failure but rather a reflection of the complex biology of CYP17A1. The dual activities of this enzyme are thought to depend on subtle conformational states and allosteric regulation by the redox partner cytochrome b_5, which is essential for lyase but not hydroxylase activity. The unique binding pose adopted by DT, while perhaps not the most thermodynamically stable, may be optimally positioned to disrupt the specific protein dynamics or substrate reorientation required for the C17-C20 bond cleavage, while not interfering with the initial hydroxylation step. The simulations also revealed a preference for a shorter, less variable hydrogen bond for dihydrotanshinone I and tanshinone IIA compared to tanshinone I, suggesting a more persistent and stable interaction that may contribute to their inhibitory mechanism. This 'function-over-affinity' hypothesis provides a powerful framework for future structure-based drug design, suggesting that optimizing for a specific inhibitory geometry, rather than raw binding energy, will be the key to enhancing potency and selectivity.

This selective inhibition profile of the tanshinones, particularly DT, represents a major pharmacological advancement over the current clinical standard, abiraterone. Abiraterone's blunt instrument approach, which potently inhibits both the 17α-hydroxylase and 17,20-lyase activities, necessitates co-administration with exogenous glucocorticoids to prevent the serious side effects of hypocortisolism and mineralocorticoid excess. The capacity of DT to spare the 17α-hydroxylase function, thereby maintaining cortisol production, could obviate the need for glucocorticoid co-therapy, a profound clinical advantage for the long-term management of chronic, non-malignant conditions like polycystic ovary syndrome (PCOS) and congenital adrenal hyperplasia.

Furthermore, the study provides a deeper understanding of the compound's mechanism of action by analyzing its effects on the off-target enzyme, CYP21A2. The data shows that while abiraterone significantly inhibits CYP21A2 activity, DT causes only a modest inhibition. The Western blot analysis provides a crucial piece of mechanistic evidence: the observed inhibition of CYP21A2 activity occurs in the absence of a decrease in protein

expression. In fact, treatment with DT and TAII led to a slight increase in CYP21A2 protein levels. This finding definitively rules out a mechanism of inhibition based on transcriptional or translational downregulation and strongly supports a direct, catalytic inhibition of the enzyme. The slight upregulation of the protein may represent a compensatory cellular feedback loop, where the cell attempts to increase enzyme synthesis to overcome the direct catalytic block.

The inhibitory action of SM extract on CYP17A1 observed in our in vitro assays appears to conflict with some in vivo studies reporting that *SM* can restore or even enhance steroidogenesis and testosterone levels. This discrepancy is not uncommon with natural products and may be explained by several factors. First, the net effect in vivo is the sum of complex systemic, hormonal, and metabolic feedback not present in a purified enzyme assay. Second, dose-dependency is a hallmark of phytopharmaceuticals; low systemic doses might have a trophic or signaling effect, while the higher concentrations used here for direct enzyme assays are inhibitory. Finally, crude extracts contain hundreds of compounds, and it is possible that other constituents have opposing, upregulating effects that dominate in a whole-organism context. The present study clarifies that the tanshinone components are, in fact, direct inhibitors.

The cytotoxicity exhibited by all tested compounds in the low micromolar range presents a dual consideration. In the context of prostate cancer, where tanshinones have been studied for their anti-proliferative effects, this cytotoxicity could be a therapeutically beneficial feature, contributing to tumor cell killing via mechanisms independent of androgen suppression [52,71–82]. These compounds could serve as alternatives or adjuncts to existing therapies, maintaining effective androgen suppression while minimizing endocrine side effects [52,74]. However, for chronic, non-lethal conditions like congenital adrenal hyperplasia and PCOS, this cytotoxicity defines the therapeutic index. Moreover, as excessive androgen production in congenital adrenal hyperplasia and PCOS worsens metabolic and reproductive dysfunction, selective lyase inhibition could normalize androgen levels without impairing cortisol or aldosterone synthesis, thereby improving patient outcomes and adherence [83,84]. The ideal drug would have a wide margin between the effective concentration for enzyme inhibition and the concentration that induces cell death. While DT emerges as a highly promising lead, our comprehensive preclinical assessment highlights that the tanshinone scaffold is a double-edged sword [73,85–87]. The very chemical features that may contribute to its bioactivity, namely the reactive quinone moiety, are also flagged by PAINS and Brenk alerts and are likely contributors to the observed cytotoxicity and the predicted liabilities of broad-spectrum CYP inhibition and immunotoxicity (Tables 3 and 4). However, use of SM in traditional medicine has a long and well tolerated safety profile and DT itself has been extensively studied [40–44,47–49,88–98]. These findings are not a disqualification but rather a critical roadmap for the next stage of development. They define the essential task for a future medicinal chemistry campaign: to systematically modify the tanshinone core to disentangle the desired on-target pharmacology from the off-target liabilities. This could involve, for example, isosteric replacement of the quinone system to reduce reactivity while preserving the geometry required for selective interaction with the CYP17A1 active site [99].

5. Conclusions

We have identified and characterized dihydrotanshinone as a potent and selective natural product-based inhibitor of CYP17A1 17,20-lyase. Its ability to suppress androgen synthesis while sparing both the critical 17α-hydroxylase function and the off-target enzyme CYP21A2 offers a significant conceptual advantage over existing non-selective inhibitors. Our integrated experimental and computational approach resolved a key structure–activity

paradox, generating the hypothesis that dihydrotanshinone's unique binding orientation, rather than its absolute binding affinity, is the primary determinant of its superior and selective function. Dihydrotanshinone therefore stands as a validated lead scaffold, providing a robust foundation for a targeted medicinal chemistry program aimed at developing a new generation of safer, more effective therapeutics for the treatment of PCOS, congenital adrenal hyperplasia, and other disorders of androgen excess.

Supplementary Materials: The following supporting information can be downloaded at https://www.mdpi.com/article/10.3390/biom16010144/s1, Figure S1: Original Western blot images.

Author Contributions: K.L.: assays, data analysis, writing. J.Y.: assays, data analysis, writing. F.S.J.: computational chemistry, data analysis, writing, consultation. A.V.P.: conceptualization, project supervision, coordination, data analysis, writing. All authors have read and agreed to the published version of the manuscript.

Funding: This research was supported by CANCER RESEARCH SWITZERLAND grant number KFS-5557-02-2022 to A.V.P. J.Y. was partially funded by a SWISS GOVERNMENT EXCELLENCE SCHOLARSHIP (ESKAS) grant number 2022.0470.

Institutional Review Board Statement: Not applicable.

Informed Consent Statement: Not applicable.

Data Availability Statement: The data that support the findings of this study are openly available Harvard Dataverse at https://doi.org/10.7910/DVN/YMX0MN (accessed on 1 January 2026) [100].

Acknowledgments: The authors acknowledge the use of Gemini 3.0 (Google) during the preparation of this manuscript. This tool was used for the purpose of correcting language and grammar to improve the clarity and readability of the text. The authors reviewed and edited all AI-generated content and take full responsibility for the integrity and accuracy of the final publication.

Conflicts of Interest: The authors declare no conflicts of interest. The funders had no role in the design of the study; in the collection, analyses, or interpretation of data; in the writing of the manuscript; or in the decision to publish the results.

References

1. Hatoum, S.; Amiri, M.; Hopkins, D.; Buyalos, R.P.; Bril, F.; Azziz, R. Population-Based vs Health System and Insurer Records: Significant Underdiagnosis of PCOS. *J. Clin. Endocrinol. Metab.* **2025**, *110*, e1759–e1766. [CrossRef]
2. Stener-Victorin, E.; Deng, Q. Epigenetic inheritance of PCOS by developmental programming and germline transmission. *Trends Endocrinol. Metab.* **2025**, *36*, 472–481. [CrossRef]
3. Helvaci, N.; Yildiz, B.O. Polycystic ovary syndrome as a metabolic disease. *Nat. Rev. Endocrinol.* **2025**, *21*, 230–244. [CrossRef]
4. Miller, W.L.; Auchus, R.J. The molecular biology, biochemistry, and physiology of human steroidogenesis and its disorders. *Endocr. Rev.* **2011**, *32*, 81–151. [CrossRef] [PubMed]
5. Vasaitis, T.S.; Bruno, R.D.; Njar, V.C. CYP17 inhibitors for prostate cancer therapy. *J. Steroid Biochem. Mol. Biol.* **2011**, *125*, 23–31. [CrossRef]
6. Pandey, A.V.; Miller, W.L. Regulation of 17,20 lyase activity by cytochrome b5 and by serine phosphorylation of P450c17. *J. Biol. Chem.* **2005**, *280*, 13265–13271. [CrossRef] [PubMed]
7. Pandey, A.V.; Mellon, S.H.; Miller, W.L. Protein phosphatase 2A and phosphoprotein SET regulate androgen production by P450c17. *J. Biol. Chem.* **2003**, *278*, 2837–2844. [CrossRef] [PubMed]
8. Zhang, L.H.; Rodriguez, H.; Ohno, S.; Miller, W.L. Serine phosphorylation of human P450c17 increases 17,20-lyase activity: Implications for adrenarche and the polycystic ovary syndrome. *Proc. Natl. Acad. Sci. USA* **1995**, *92*, 10619–10623. [CrossRef]
9. Tee, M.K.; Miller, W.L. Phosphorylation of human cytochrome P450c17 by p38alpha selectively increases 17,20 lyase activity and androgen biosynthesis. *J. Biol. Chem.* **2013**, *288*, 23903–23913. [CrossRef]
10. Huynh, T.; McGown, I.; Cowley, D.; Nyunt, O.; Leong, G.M.; Harris, M.; Cotterill, A.M. The Clinical and Biochemical Spectrum of Congenital Adrenal Hyperplasia Secondary to 21-Hydroxylase Deficiency. *Clin. Biochem. Rev.* **2009**, *30*, 75–86.

11. Nimkarn, S.; Gangishetti, P.K.; Yau, M.; New, M.I. 21-Hydroxylase-Deficient Congenital Adrenal Hyperplasia. In *GeneReviews®*; Adam, M.P., Feldman, J., Mirzaa, G.M., Pagon, R.A., Wallace, S.E., Amemiya, A., Eds.; University of Washington: Seattle WA, USA, 1993.
12. Lord, J.M.; Flight, I.H.K.; Norman, R.J. Metformin in polycystic ovary syndrome: Systematic review and meta-analysis. *BMJ Br. Med. J.* **2003**, *327*, 951. [CrossRef]
13. Lidegaard, Ø.; Løkkegaard, E.; Jensen, A.; Skovlund, C.W.; Keiding, N. Thrombotic Stroke and Myocardial Infarction with Hormonal Contraception. *N. Engl. J. Med.* **2012**, *366*, 2257–2266. [CrossRef]
14. Vitale, S.G.; Di Michele, S.; Tassi, A.; Succu, C.; Angioni, S.; Fulghesu, A.M. Sustained Metabolic Improvements with Low-Dose Metformin Combined with Oral Contraceptives in Female Adolescents with PCOS: A Single-Center Retrospective Cohort Study. *Adv. Ther.* **2025**, *42*, 3762–3773. [CrossRef]
15. Wrobel, T.M.; Grudzinska, A.; Yakubu, J.; du Toit, T.; Sharma, K.; Harrington, J.C.; Bjorkling, F.; Jorgensen, F.S.; Pandey, A.V. Pyridine indole hybrids as novel potent CYP17A1 inhibitors. *J. Enzym. Inhib. Med. Chem.* **2025**, *40*, 2463014. [CrossRef]
16. Wrobel, T.M.; Jorgensen, F.S.; Pandey, A.V.; Grudzinska, A.; Sharma, K.; Yakubu, J.; Bjorkling, F. Non-steroidal CYP17A1 Inhibitors: Discovery and Assessment. *J. Med. Chem.* **2023**, *66*, 6542–6566. [CrossRef] [PubMed]
17. Wrobel, T.M.; Rogova, O.; Sharma, K.; Rojas Velazquez, M.N.; Pandey, A.V.; Jorgensen, F.S.; Arendrup, F.S.; Andersen, K.L.; Bjorkling, F. Synthesis and Structure-Activity Relationships of Novel Non-Steroidal CYP17A1 Inhibitors as Potential Prostate Cancer Agents. *Biomolecules* **2022**, *12*, 165. [CrossRef]
18. Wrobel, T.M.; Rogova, O.; Andersen, K.L.; Yadav, R.; Brixius-Anderko, S.; Scott, E.E.; Olsen, L.; Jorgensen, F.S.; Bjorkling, F. Discovery of Novel Non-Steroidal Cytochrome P450 17A1 Inhibitors as Potential Prostate Cancer Agents. *Int. J. Mol. Sci.* **2020**, *21*, 4868. [CrossRef] [PubMed]
19. Munkboel, C.H.; Christensen, L.R.; Islin, J.; Bonomo, S.; Olsen, L.; Jorgensen, F.S.; Styrishave, B. The anti-epileptic drug lamotrigine inhibits the CYP17A1 lyase reaction in vitro. *Biol. Reprod.* **2018**, *99*, 888–897. [CrossRef]
20. Larsen, M.; Hansen, C.H.; Rasmussen, T.B.; Islin, J.; Styrishave, B.; Olsen, L.; Jorgensen, F.S. Structure-based optimisation of non-steroidal cytochrome P450 17A1 inhibitors. *Chem. Commun.* **2017**, *53*, 3118–3121. [CrossRef] [PubMed]
21. de Bono, J.S.; Logothetis, C.J.; Molina, A.; Fizazi, K.; North, S.; Chu, L.; Chi, K.N.; Jones, R.J.; Goodman, O.B.; Saad, F.; et al. Abiraterone and Increased Survival in Metastatic Prostate Cancer. *N. Engl. J. Med.* **2011**, *364*, 1995–2005. [CrossRef]
22. Attard, G.; Reid, A.H.M.; Auchus, R.J.; Hughes, B.A.; Cassidy, A.M.; Thompson, E.; Oommen, N.B.; Folkerd, E.; Dowsett, M.; Arlt, W.; et al. Clinical and biochemical consequences of CYP17A1 inhibition with abiraterone given with and without exogenous glucocorticoids in castrate men with advanced prostate cancer. *J. Clin. Endocrinol. Metab.* **2012**, *97*, 507–516. [CrossRef]
23. Ryan, C.J.; Smith, M.R.; de Bono, J.S.; Molina, A.; Logothetis, C.J.; de Souza, P.; Fizazi, K.; Mainwaring, P.; Piulats, J.M.; Ng, S.; et al. Randomized Phase 3 Trial of Abiraterone Acetate in Men with Metastatic Castration-Resistant Prostate Cancer and No Prior Chemotherapy. *N. Engl. J. Med.* **2013**, *368*, 138–148. [CrossRef] [PubMed]
24. Malikova, J.; Brixius-Anderko, S.; Udhane, S.S.; Parween, S.; Dick, B.; Bernhardt, R.; Pandey, A.V. CYP17A1 inhibitor abiraterone, an anti-prostate cancer drug, also inhibits the 21-hydroxylase activity of CYP21A2. *J. Steroid Biochem. Mol. Biol.* **2017**, *174*, 192–200. [CrossRef] [PubMed]
25. Udhane, S.S.; Dick, B.; Hu, Q.; Hartmann, R.W.; Pandey, A.V. Specificity of anti-prostate cancer CYP17A1 inhibitors on androgen biosynthesis. *Biochem. Biophys. Res. Commun.* **2016**, *477*, 1005–1010. [CrossRef] [PubMed]
26. Fehl, C.; Vogt, C.D.; Yadav, R.; Li, K.; Scott, E.E.; Aubé, J. Structure-Based Design of Inhibitors with Improved Selectivity for Steroidogenic Cytochrome P450 17A1 over Cytochrome P450 21A2. *J. Med. Chem.* **2018**, *61*, 4946. [CrossRef]
27. McCrea, E.; Sissung, T.M.; Price, D.K.; Chau, C.H.; Figg, W.D. Androgen receptor variation affects prostate cancer progression and drug resistance. *Pharmacol. Res.* **2016**, *114*, 152–162. [CrossRef]
28. Yakubu, J.; Natsaridis, E.; du Toit, T.; Barata, I.S.; Tagit, O.; Pandey, A.V. Nanoparticles with curcumin and piperine modulate steroid biosynthesis in prostate cancer. *Sci. Rep.* **2025**, *15*, 13613. [CrossRef]
29. Sharma, K.; Lanzilotto, A.; Yakubu, J.; Therkelsen, S.; Voegel, C.D.; Du Toit, T.; Jorgensen, F.S.; Pandey, A.V. Effect of Essential Oil Components on the Activity of Steroidogenic Cytochrome P450. *Biomolecules* **2024**, *14*, 203. [CrossRef]
30. Mayr, F.; Moller, G.; Garscha, U.; Fischer, J.; Rodriguez Castano, P.; Inderbinen, S.G.; Temml, V.; Waltenberger, B.; Schwaiger, S.; Hartmann, R.W.; et al. Finding New Molecular Targets of Familiar Natural Products Using In Silico Target Prediction. *Int. J. Mol. Sci.* **2020**, *21*, 7102. [CrossRef]
31. Rodríguez Castaño, P.; Parween, S.; Pandey, A.V. Bioactivity of Curcumin on the Cytochrome P450 Enzymes of the Steroidogenic Pathway. *Int. J. Mol. Sci.* **2019**, *20*, 4606. [CrossRef]
32. Sethi, K.K.; Sahoo, S.K.; Pichikala, J.N.; Suresh, P. Carbonic anhydrase I and II inhibition with natural products: Caffeine and piperine. *J. Enzym. Inhib. Med. Chem.* **2012**, *27*, 97–100. [CrossRef] [PubMed]
33. Sahin, H.; Can, Z.; Yildiz, O.; Kolayli, S.; Innocenti, A.; Scozzafava, G.; Supuran, C.T. Inhibition of carbonic anhydrase isozymes I and II with natural products extracted from plants, mushrooms and honey. *J. Enzym. Inhib. Med. Chem.* **2012**, *27*, 395–402. [CrossRef]

34. Mukanganyama, S.; Bezabih, M.; Robert, M.; Ngadjui, B.T.; Kapche, G.F.; Ngandeu, F.; Abegaz, B. The evaluation of novel natural products as inhibitors of human glutathione transferase P1-1. *J. Enzym. Inhib. Med. Chem.* **2011**, *26*, 460–467. [CrossRef]
35. Liu, J.Y.; Guo, H.Y.; Quan, Z.S.; Shen, Q.K.; Cui, H.; Li, X. Research progress of natural products and their derivatives against Alzheimer's disease. *J. Enzym. Inhib. Med. Chem.* **2023**, *38*, 2171026. [CrossRef]
36. Sultana, N. Clinically useful anticancer, antitumor, and antiwrinkle agent, ursolic acid and related derivatives as medicinally important natural product. *J. Enzym. Inhib. Med. Chem.* **2011**, *26*, 616–642. [CrossRef]
37. Babhare, A.; Nandurkar, D.; Danao, K.; Warokar, A.; Mahajan, U. Exploration of Herbal Medicinal Plants and Formulations Available for the Treatment of PCOS: A review. *JBRA Assist. Reprod.* **2025**, *29*, 367–377. [CrossRef]
38. Su, P.; Wang, X.; Cai, R.; Yan, C.; Sun, Y. Effects of cryptotanshinone in treatment of polycystic ovary syndrome in rats: A systematic review and meta-analysis. *Front. Pharmacol.* **2025**, *16*, 1561164. [CrossRef]
39. Yuan, J.; Li, Z.; Yu, Y.; Wang, X.; Zhao, Y. Natural compounds in the management of polycystic ovary syndrome: A comprehensive review of hormonal regulation and therapeutic potential. *Front. Nutr.* **2025**, *12*, 1520695. [CrossRef] [PubMed]
40. Shi, W.; Wen, J.; Gao, Y.; Liu, T.; Li, H.; Yang, H.; Zhao, J.; Wei, Z.; Li, C.; Yao, Q.; et al. Dihydrotanshinone I, a main compound of Salvia miltiorrhiza, alleviates autoimmune and inflammatory diseases by directly targeting IRF3. *Phytomedicine* **2025**, *145*, 157005. [CrossRef]
41. Li, A.; Yang, M.; Duan, W.; Wu, B. Dihydrotanshinone I induces necroptosis and cell cycle arrest in gastric cancer through the PTPN11/p38 pathway. *Toxicol. Vitr.* **2025**, *102*, 105955. [CrossRef] [PubMed]
42. Han, B.; Sun, C.; Yang, R.; Li, X.; Kang, J.; Cai, J.; Zhou, S.; Wang, G.; Wang, J.; Zhang, J.; et al. Dihydrotanshinone I inhibits ovarian tumor growth by suppressing ITGB1/FAK-mediated extracellular matrix signaling. *Phytomedicine* **2025**, *145*, 157023. [CrossRef]
43. Dev, A.J.R.; Malhotra, L.; Kashyap, A.; Umar, S.M.; Rathee, M.; Samanta, S.; Kharkwal, R.; Sengupta, D.; Prasad, C.P. Biophysical and molecular characterization of HuR inhibitors, CMLD-2 and Dihydrotanshinone I (DHTS), in Triple Negative Breast Cancer (TNBC). *Int. J. Biol. Macromol.* **2025**, *320*, 145848. [CrossRef] [PubMed]
44. Yue, J.; Hao, D.; Wang, Y.; Guo, J.; Liu, S.; Meng, L.; Liu, J. The multifaceted mechanisms of Dihydrotanshinone I in the treatment of tumors. *Biomed. Pharmacother.* **2024**, *175*, 116635. [CrossRef]
45. Shen, W.; Jin, B.; Pan, Y.; Han, Y.; You, T.; Zhang, Z.; Qu, Y.; Liu, S.; Zhang, Y. The Effects of Traditional Chinese Medicine-Associated Complementary and Alternative Medicine on Women with Polycystic Ovary Syndrome. *Evid.-Based Complement. Altern. Med. eCAM* **2021**, *2021*, 6619597. [CrossRef] [PubMed]
46. Chen, H.; Deng, C.; Meng, Z.; Meng, S. Effects of TCM on polycystic ovary syndrome and its cellular endocrine mechanism. *Front. Endocrinol.* **2023**, *14*, 956772. [CrossRef] [PubMed]
47. Zhang, Y.Z.; Wei, Z.J.; Yu, S.N.; Wang, X.Y.; Wang, Y.; Wu, C.A.; Jiang, X. Dihydrotanshinone I protects human chondrocytes and alleviates damage from spontaneous osteoarthritis in a guinea pig model. *Sci. Rep.* **2023**, *13*, 21355. [CrossRef]
48. Shen, N.; Li, M.; Fang, B.; Li, X.; Jiang, F.; Zhu, T.; Zheng, J.; Zhang, W. ALOX15-Driven Ferroptosis: The key target in Dihydrotanshinone I's epigenetic Battle in hepatic stellate cells against liver fibrosis. *Int. Immunopharmacol.* **2025**, *146*, 113827. [CrossRef]
49. Molteni, E.; Baldan, F.; Damante, G.; Allegri, L. Dihydrotanshinone I exhibits antitumor effects via beta-catenin downregulation in papillary thyroid cancer cell lines. *Sci. Rep.* **2024**, *14*, 7853. [CrossRef]
50. Hsu, Y.C.; Shih, Y.H.; Ho, C.; Liu, C.C.; Liaw, C.C.; Lin, H.Y.; Lin, C.L. Ethyl Acetate Fractions of Salvia miltiorrhiza Bunge (Danshen) Crude Extract Modulate Fibrotic Signals to Ameliorate Diabetic Kidney Injury. *Int. J. Mol. Sci.* **2024**, *25*, 8986. [CrossRef]
51. Heidarzadehpilehrood, R.; Pirhoushiaran, M.; Abdollahzadeh, R.; Binti Osman, M.; Sakinah, M.; Nordin, N.; Abdul Hamid, H. A Review on CYP11A1, CYP17A1, and CYP19A1 Polymorphism Studies: Candidate Susceptibility Genes for Polycystic Ovary Syndrome (PCOS) and Infertility. *Genes* **2022**, *13*, 302. [CrossRef]
52. Ji, X.Z.; Qin, X.; Wang, W.; Wang, L. A review of tanshinone compounds in prostate cancer treatment. *Transl. Androl. Urol.* **2024**, *13*, 1278–1287. [CrossRef]
53. Rojas Velazquez, M.N.; Lopez Dacal, J.; Jørgensen, F.S.; Sanguineti, N.; Sharma, K.; Marino, R.; Garrido, N.P.; Vaiani, E.; Ramírez, P.; Scaglia, P.; et al. A novel POR G88S mutation causes severe PORD and establishes a critical pharmacogenomic risk profile. *J. Clin. Endocrinol. Metab.* **2025**, dgaf630. [CrossRef] [PubMed]
54. Prado, M.J.; Singh, S.; Ligabue-Braun, R.; Meneghetti, B.V.; Rispoli, T.; Kopacek, C.; Monteiro, K.; Zaha, A.; Rossetti, M.L.R.; Pandey, A.V. Characterization of Mutations Causing CYP21A2 Deficiency in Brazilian and Portuguese Populations. *Int. J. Mol. Sci.* **2021**, *23*, 296. [CrossRef]
55. Sastry, G.M.; Adzhigirey, M.; Day, T.; Annabhimoju, R.; Sherman, W. Protein and ligand preparation: Parameters, protocols, and influence on virtual screening enrichments. *J. Comput. Aided Mol. Des.* **2013**, *27*, 221–234. [CrossRef]
56. Kim, S.; Chen, J.; Cheng, T.; Gindulyte, A.; He, J.; He, S.; Li, Q.; Shoemaker, B.A.; Thiessen, P.A.; Yu, B.; et al. PubChem 2025 update. *Nucleic Acids Res.* **2025**, *53*, D1516–D1525. [CrossRef]

57. Berman, H.M.; Westbrook, J.; Feng, Z.; Gilliland, G.; Bhat, T.N.; Weissig, H.; Shindyalov, I.N.; Bourne, P.E. The Protein Data Bank. *Nucleic Acids Res.* **2000**, *28*, 235–242. [CrossRef] [PubMed]
58. Petrunak, E.M.; Rogers, S.A.; Aube, J.; Scott, E.E. Structural and Functional Evaluation of Clinically Relevant Inhibitors of Steroidogenic Cytochrome P450 17A1. *Drug Metab. Dispos.* **2017**, *45*, 635–645. [CrossRef]
59. Petrunak, E.M.; DeVore, N.M.; Porubsky, P.R.; Scott, E.E. Structures of human steroidogenic cytochrome P450 17A1 with substrates. *J. Biol. Chem.* **2014**, *289*, 32952–32964. [CrossRef] [PubMed]
60. Chen, Y.C. Beware of docking! *Trends Pharmacol. Sci.* **2015**, *36*, 78–95. [CrossRef] [PubMed]
61. Genheden, S.; Ryde, U. The MM/PBSA and MM/GBSA methods to estimate ligand-binding affinities. *Expert Opin. Drug Discov.* **2015**, *10*, 449–461. [CrossRef]
62. Wang, E.; Sun, H.; Wang, J.; Wang, Z.; Liu, H.; Zhang, J.Z.H.; Hou, T. End-Point Binding Free Energy Calculation with MM/PBSA and MM/GBSA: Strategies and Applications in Drug Design. *Chem. Rev.* **2019**, *119*, 9478–9508. [CrossRef] [PubMed]
63. Pantsar, T.; Poso, A. Binding Affinity via Docking: Fact and Fiction. *Molecules* **2018**, *23*, 1899. [CrossRef]
64. Siebenmorgen, T.; Zacharias, M. Efficient Refinement and Free Energy Scoring of Predicted Protein-Protein Complexes Using Replica Exchange with Repulsive Scaling. *J. Chem. Inf. Model.* **2020**, *60*, 5552–5562. [CrossRef]
65. Kairys, V.; Baranauskiene, L.; Kazlauskiene, M.; Matulis, D.; Kazlauskas, E. Binding affinity in drug design: Experimental and computational techniques. *Expert Opin. Drug Discov.* **2019**, *14*, 755–768. [CrossRef]
66. Daina, A.; Michielin, O.; Zoete, V. SwissADME: A free web tool to evaluate pharmacokinetics, drug-likeness and medicinal chemistry friendliness of small molecules. *Sci. Rep.* **2017**, *7*, 42717. [CrossRef]
67. Banerjee, P.; Kemmler, E.; Dunkel, M.; Preissner, R. ProTox 3.0: A webserver for the prediction of toxicity of chemicals. *Nucleic Acids Res.* **2024**, *52*, W513–W520. [CrossRef]
68. Olsen, L.; Montefiori, M.; Tran, K.P.; Jorgensen, F.S. SMARTCyp 3.0: Enhanced cytochrome P450 site-of-metabolism prediction server. *Bioinformatics* **2019**, *35*, 3174–3175. [CrossRef]
69. Olsen, L.; Oostenbrink, C.; Jorgensen, F.S. Prediction of cytochrome P450 mediated metabolism. *Adv. Drug Deliv. Rev.* **2015**, *86*, 61–71. [CrossRef]
70. Bonomo, S.; Jorgensen, F.S.; Olsen, L. Mechanism of Cytochrome P450 17A1-Catalyzed Hydroxylase and Lyase Reactions. *J. Chem. Inf. Model.* **2017**, *57*, 1123–1133. [CrossRef] [PubMed]
71. Yu, J.; Li, S.; Cheng, S.; Ahmad, M.; Chen, C.; Wan, X.; Wei, S.; Pan, W.; Luo, H. Tanshinone analog inhibits castration-resistant prostate cancer cell growth by inhibiting glycolysis in an AR-dependent manner. *J. Biol. Chem.* **2024**, *300*, 107139. [CrossRef] [PubMed]
72. Zhang, T.; Chen, X.; Ju, X.; Yuan, J.; Zhou, J.; Zhang, Z.; Ju, G.; Xu, D. PPARG is a potential target of Tanshinone IIA in prostate cancer treatment: A combination study of molecular docking and dynamic simulation based on transcriptomic bioinformatics. *Eur. J. Med. Res.* **2023**, *28*, 487. [CrossRef] [PubMed]
73. Shakeri, A.; Hafezian, T.; Kusz, N.; Hohmann, J.; Boozari, M.; Mottaghipisheh, J.; Emami, S.A.; Tayarani-Najaran, Z.; Asili, J. Cytotoxicity, apoptosis inducing activity and Western blot analysis of tanshinone derivatives from Stachys parviflora on prostate and breast cancer cells. *Mol. Biol. Rep.* **2022**, *49*, 8251–8258. [CrossRef]
74. Li, W.; Huang, T.; Xu, S.; Che, B.; Yu, Y.; Zhang, W.; Tang, K. Molecular Mechanism of Tanshinone against Prostate Cancer. *Molecules* **2022**, *27*, 5594. [CrossRef]
75. Sun, G.; Sun, K.; Sun, J. Combination prostate cancer therapy: Prostate-specific membranes antigen targeted, pH-sensitive nanoparticles loaded with doxorubicin and tanshinone. *Drug Deliv.* **2021**, *28*, 1132–1140. [CrossRef]
76. Wu, C.Y.; Yang, Y.H.; Lin, Y.Y.; Kuan, F.C.; Lin, Y.S.; Lin, W.Y.; Tsai, M.Y.; Yang, J.J.; Cheng, Y.C.; Shu, L.H.; et al. Anti-cancer effect of danshen and dihydroisotanshinone I on prostate cancer: Targeting the crosstalk between macrophages and cancer cells via inhibition of the STAT3/CCL2 signaling pathway. *Oncotarget* **2017**, *8*, 40246–40263. [CrossRef]
77. Li, C.; Han, X.; Zhang, H.; Wu, J.; Li, B. The interplay between autophagy and apoptosis induced by tanshinone IIA in prostate cancer cells. *Tumour Biol.* **2016**, *37*, 7667–7674. [CrossRef]
78. Ketola, K.; Viitala, M.; Kohonen, P.; Fey, V.; Culig, Z.; Kallioniemi, O.; Iljin, K. High-throughput cell-based compound screen identifies pinosylvin methyl ether and tanshinone IIA as inhibitors of castration-resistant prostate cancer. *J. Mol. Biochem.* **2016**, *5*, 12–22.
79. Chiu, S.C.; Huang, S.Y.; Chen, S.P.; Su, C.C.; Chiu, T.L.; Pang, C.Y. Tanshinone IIA inhibits human prostate cancer cells growth by induction of endoplasmic reticulum stress in vitro and in vivo. *Prostate Cancer Prostatic Dis.* **2013**, *16*, 315–322. [CrossRef] [PubMed]
80. Won, S.H.; Lee, H.J.; Jeong, S.J.; Lu, J.; Kim, S.H. Activation of p53 signaling and inhibition of androgen receptor mediate tanshinone IIA induced G1 arrest in LNCaP prostate cancer cells. *Phytother. Res. PTR* **2012**, *26*, 669–674. [CrossRef]
81. Liu, W.; Zhou, J.; Geng, G.; Shi, Q.; Sauriol, F.; Wu, J.H. Antiandrogenic, maspin induction, and antiprostate cancer activities of tanshinone IIA and its novel derivatives with modification in ring A. *J. Med. Chem.* **2012**, *55*, 971–975. [CrossRef] [PubMed]

82. Won, S.H.; Lee, H.J.; Jeong, S.J.; Lee, H.J.; Lee, E.O.; Jung, D.B.; Shin, J.M.; Kwon, T.R.; Yun, S.M.; Lee, M.H.; et al. Tanshinone IIA induces mitochondria dependent apoptosis in prostate cancer cells in association with an inhibition of phosphoinositide 3-kinase/AKT pathway. *Biol. Pharm. Bull.* **2010**, *33*, 1828–1834. [CrossRef] [PubMed]
83. Escobar-Morreale, H.F. Polycystic ovary syndrome: Definition, aetiology, diagnosis and treatment. *Nat. Rev. Endocrinol.* **2018**, *14*, 270–284. [CrossRef]
84. Goodarzi, M.O.; Dumesic, D.A.; Chazenbalk, G.; Azziz, R. Polycystic ovary syndrome: Etiology, pathogenesis and diagnosis. *Nat. Rev. Endocrinol.* **2011**, *7*, 219–231. [CrossRef]
85. Li, S.; Teng, F.; Zhang, J.; Zhang, P.; Li, M.; Wang, X.; Li, K. Tanshinone IIA potentiates the chemotherapeutic effect of doxorubicin against breast cancer cells and attenuates the cardiotoxicity of doxorubicin by regulating ERK1/2 pathway. *J. Biochem. Mol. Toxicol.* **2024**, *38*, e23851. [CrossRef] [PubMed]
86. Fengchao, C.; Siya, Z.; Tongtong, Y.; Hongquan, W.; Jie, L.; Qiang, W.; Danish, S.; Kun, L. The enhanced cytotoxicity on breast cancer cells by Tanshinone I-induced photodynamic effect. *Sci. Rep.* **2023**, *13*, 18107. [CrossRef] [PubMed]
87. Lin, H.; Zheng, L.; Li, S.; Xie, B.; Cui, B.; Xia, A.; Lin, Z.; Zhou, P. Cytotoxicity of Tanshinone IIA combined with Taxol on drug-resist breast cancer cells MCF-7 through inhibition of Tau. *Phytother. Res. PTR* **2018**, *32*, 667–671. [CrossRef]
88. Dai, S.; Ding, Y.; Guo, J.; Wang, X. Efficacy and safety of danshen class injections in the treatment of coronary heart disease: A network meta-analysis. *Front. Pharmacol.* **2024**, *15*, 1487119. [CrossRef]
89. Zhu, R.R.; Zhou, X.L.; Liu, Y.W.; Xu, R.; Deng, P.; Liu, Z.Y. Engineered endothelial cells targeting and dihydrotanshinone I loaded bacterial extracellular vesicles for atherosclerosis therapy. *Bioeng. Transl. Med.* **2025**, *10*, e70074. [CrossRef]
90. Xu, R.; Dai, J.; Gong, R.; Tu, R.; Wang, Q.; Zheng, H.; Zhou, L.; Wang, S.; Cai, J.; Sun, H.; et al. Dihydrotanshinone I Targets PGAM1 to Induce SYVN1-Mediated Ubiquitination and Suppress Glycolysis in Hepatocellular Carcinoma. *Phytother. Res. PTR* **2025**, *39*, 3762–3783. [CrossRef]
91. Mahendran, R.; Lim, S.K.; Ong, K.C.; Chua, K.H.; Chai, H.C. Antiproliferative effects of dihydrotanshinone I on autosomal dominant polycystic kidney disease via immunomodulation. *J. Pharmacol. Exp. Ther.* **2025**, *392*, 103655. [CrossRef]
92. Luo, X.; Duan, Y.; He, J.; Huang, C.; Liu, J.; Liu, Y.; Xu, M.; Dai, Q.; Yang, Z. Dihydrotanshinone I enhanced BRAF mutant melanoma treatment efficacy by inhibiting the STAT3/SOX2 signaling pathway. *Front. Oncol.* **2025**, *15*, 1429018. [CrossRef] [PubMed]
93. Lin, H.; Sui, H.; Yu, Y.; Xie, C.; Shen, Y.; Cheng, L.; Wang, J.; Yu, Y.; Xie, C.; Cui, R. Dihydrotanshinone I potentiates the anti-tumor activity of cisplatin by activating ROS-mediated ER stress through targeting HSPD1 in lung cancer cells. *Eur. J. Pharmacol.* **2025**, *994*, 177378. [CrossRef]
94. Huang, X.; Huang, L.; Ni, X.; Wang, Q.Q.; Liu, L.; Shen, Y.; Xiao, L.; Yang, S.; Yuan, R.; Li, X.X.; et al. Dihydrotanshinone Alleviates Lipopolysaccharide-Induced Acute Lung Injury by Targeting NEK7 to Inhibit NLRP3 Inflammasome Activation. *Phytother. Res.* **2025**. [CrossRef] [PubMed]
95. Wang, X.; Jing, Z.; Huang, X.; Liu, X.; Zhang, Y.; Wang, Z.; Ma, P. PD-L1 antibody conjugated dihydrotanshinone I-loaded polymeric nanoparticle for targeted cancer immunotherapy combining PD-L1 blockade with immunogenic cell death. *Int. J. Pharm.* **2024**, *667*, 125004. [CrossRef]
96. Nie, Y.; Yan, J.; Huang, X.; Jiang, T.; Zhang, S.; Zhang, G. Dihydrotanshinone I targets ESR1 to induce DNA double-strand breaks and proliferation inhibition in hepatocellular carcinoma. *Phytomedicine* **2024**, *130*, 155767. [CrossRef] [PubMed]
97. Muroi, M.; Lee, D.S. Inhibitory Effects of Cryptotanshinone and Dihydrotanshinone I on Intracellular Trafficking of Viral Glycoproteins. *J. Microbiol. Biotechnol.* **2024**, *34*, 2457–2464. [CrossRef] [PubMed]
98. Li, Z.; Mo, R.L.; Gong, J.F.; Han, L.; Wang, W.F.; Huang, D.K.; Xu, J.G.; Sun, Y.J.; Chen, S.; Han, G.C.; et al. Dihydrotanshinone I inhibits gallbladder cancer growth by targeting the Keap1-Nrf2 signaling pathway and Nrf2 phosphorylation. *Phytomedicine* **2024**, *129*, 155661. [CrossRef]
99. Zhang, R.H.; Guo, H.Y.; Deng, H.; Li, J.; Quan, Z.S. Piperazine skeleton in the structural modification of natural products: A review. *J. Enzym. Inhib. Med. Chem.* **2021**, *36*, 1165–1197. [CrossRef]
100. Pandey, A.V. Dataset for: Dihydrotanshinone As a Natural Product-Based CYP17A1 Lyase Inhibitor for Hyperandrogenic Disorders. *Harvard Dataverse*. 2025. Available online: https://doi.org/10.7910/DVN/YMX0MN (accessed on 1 January 2026).

Disclaimer/Publisher's Note: The statements, opinions and data contained in all publications are solely those of the individual author(s) and contributor(s) and not of MDPI and/or the editor(s). MDPI and/or the editor(s) disclaim responsibility for any injury to people or property resulting from any ideas, methods, instructions or products referred to in the content.